Mindin (SPON2) Is Essential for Cutaneous Fibrogenesis in a Mouse Model of Systemic Sclerosis

JID Open

Isha Rana[1,2,21], Sunny Kataria[1,3,21], Tuan Lin Tan[4,5,21], Edries Yousaf Hajam[1,2], Deepak Kumar Kashyap[6,7], Dyuti Saha[1,8], Johan Ajnabi[1], Sayan Paul[6], Shashank Jayappa[6], Akhil S.H.P. Ananthan[1], Pankaj Kumar[1], Rania F. Zaarour[1,9], J. Haarshaadri[1], Gaurav Kansagara[1,10], Abrar Rizvi[1], Ravindra K. Zirmire[1,2], Krithika Badarinath[1,3], Sneha Uday Khedkar[1], Yogesh Chandra[10], Rekha Samuel[11,12], Renu George[13], Debashish Danda[14], Paul Mazhuvanchary Jacob[15], Rakesh Dey[1], Perundurai S. Dhandapany[5], You-Wen He[16], John Varga[17], Shyni Varghese[4,18,19,20] and Colin Jamora[1]

Systemic sclerosis is a fibrotic disease that initiates in the skin and progresses to internal organs, leading to a poor prognosis. Unraveling the etiology of a chronic, multifactorial disease such as systemic sclerosis has been aided by various animal models that recapitulate certain aspects of the human pathology. We found that the transcription factor SNAI1 is overexpressed in the epidermis of patients with systemic sclerosis, and a transgenic mouse recapitulating this expression pattern is sufficient to induce many clinical features of the human disease. Using this mouse model as a discovery platform, we have uncovered a critical role for the matricellular protein Mindin (SPON2) in fibrogenesis. Mindin is produced by SNAI1 transgenic skin keratinocytes and aids fibrogenesis by inducing early inflammatory cytokine production and collagen secretion in resident dermal fibroblasts. Given the dispensability of Mindin in normal tissue physiology, targeting this protein holds promise as an effective therapy for fibrosis.

Journal of Investigative Dermatology (2023) **143,** 699–710; doi:10.1016/j.jid.2022.10.011

[1]*IFOM-inStem Joint Research Laboratory, Centre for Inflammation and Tissue Homeostasis, Institute for Stem Cell Science & Regenerative Medicine, Bangalore, India;* [2]*School of Chemical and Biotechnology, Shanmugha Arts, Science, Technology and Research Academy (SASTRA) Deemed University, Thanjavur, India;* [3]*National Centre for Biological Sciences, Bangalore, India;* [4]*Department of Bioengineering, Jacobs School of Engineering, University of California San Diego, San Diego, California, USA;* [5]*School of Chemical & Life Sciences, Singapore Polytechnic, Singapore, Singapore;* [6]*Centre for Cardiovascular Biology and Disease, Institute for Stem Cell Science and Regenerative Medicine, Bangalore, India;* [7]*Centre for Cellular and Molecular Biology, Hyderabad, India;* [8]*Manipal Academy of Higher Education (MAHE), Manipal, India;* [9]*Thumbay Research Institute for Precision Medicine (TRIPM), Gulf Medical University, Ajman, United Arab Emirates;* [10]*Animal Care and Resource Centre (ACRC), Bangalore Life Science Cluster, Bangalore, India;* [11]*Centre for Stem Cell Research (CSCR), Christian Medical College Vellore, Vellore, India;* [12]*Department of Pathology, Manipal - Tata Medical College Jamshedpur, Jamshedpur, India;* [13]*Department of Dermatology, Venereology and Leprosy, Christian Medical College Vellore, Vellore, India;* [14]*Department of Clinical Immunology & Rheumatology, Christian Medical College Vellore, Vellore, India;* [15]*Department of Surgery, Christian Medical College Vellore, Vellore, India;* [16]*Department of Immunology, Duke University School of Medicine, Durham, North Carolina, USA;* [17]*Department of Internal Medicine, Michigan Medicine, University of Michigan, Ann Arbor, Michigan, USA;* [18]*Department of Biomedical Engineering, Duke University, Durham, North Carolina, USA;* [19]*Department of Mechanical Engineering & Materials Science, Duke University, Durham, North Carolina, USA; and* [20]*Department of Orthopaedic Surgery, Duke University School of Medicine, Durham, North Carolina, USA*

[21]*These authors contributed equally to this work.*

Correspondence: Colin Jamora, Centre for Inflammation and Tissue Homeostasis, Institute for Stem Cell Science & Regenerative Medicine, GKVK Post, Bellary Road, Bangalore 560065, India. E-mail: colinj@instem.res.in

Abbreviations: CM, conditioned media; dSSc, diffused systemic sclerosis; KC, keratinocyte; SSc, systemic sclerosis; Tg, transgenic; WT, wild type

Received 29 March 2022; revised 2 October 2022; accepted 4 October 2022; accepted manuscript published online 15 December 2022; corrected proof published online 19 January 2023

INTRODUCTION

Tissue fibrosis is a pathological condition in which the diseased or damaged tissue is replaced by excessive extracellular matrix, leading to tissue hardening and loss of organ function. Secretion of extracellular matrix by activated fibroblasts (myofibroblasts) is a physiological response of the wound healing program. However, unlike canonical dermal wound healing, in the context of fibrosis, fibroblasts remain persistently activated and are likely sustained through positive feedback loops between fibroblast activation, inflammation (Wynn, 2008), tissue stiffness (Nakasaki et al., 2015), and vascular damage (Enzerink and Vaheri, 2011). When critical organs such as the lungs, heart, kidney, or liver become affected, the consequences of such overscarring become fatal. For this reason, fibrosis is a major contributor to many diseases and ~ 40% of mortalities worldwide (Wynn, 2007).

An example of a fibrotic disorder with a poor prognosis is scleroderma, a group of skin fibrotic disorders with different subtypes classified by the extent of tissue involvement. The subcategories of scleroderma are localized scleroderma and systemic scleroderma or systemic sclerosis (SSc). Localized scleroderma is limited to affecting only certain areas of the skin (Denton and Khanna, 2017). In contrast, SSc is a progressive fibrotic disease with inflammatory, autoimmune, and vascular defects (Van Den Hoogen et al., 2013). Fibrosis characteristically initiates in the skin of distal extremities. The skin manifestations are limited to these areas in the case of limited SSc; however, large areas of skin are involved in cases of diffused SSc (dSSc). Unlike localized scleroderma, which negatively impacts the QOL, SSc can progress to involve

critical organs such as the lungs, heart, and kidney often with fatal consequences.

A number of mouse models have been developed to understand the molecular basis of SSc and to be used as a platform for potential therapeutic development (Yue et al., 2018). The current mouse models recapitulate at least one of the clinical hallmarks of SSc, although a holistic animal model that can mimic the full spectrum and progressive nature of the human SSc disease is limited. One of these models, the Fli1+/− Klf5+/− haploinsufficiency mouse, can exhibit the later symptoms of SSc: vasculopathy, fibrosis, and the progressive involvement of internal organs (Noda et al., 2014). A mouse model that can manifest the earliest symptoms of the disease such as Raynaud-like phenomenon and puffy fingers (both indicative of vascular defects of SSc) followed by chronic inflammation, systemic autoimmunity, progressive fibrosis in the skin, and involvement of other internal organs would be a valuable tool to increase our understanding of the etiology of SSc and illuminate new ways to treat this disease.

RESULTS

The SNAI1 transgenic mouse recapitulates clinical features of scleroderma patients

In light of the upregulation of SNAI1 in multiple fibrotic tissues (Boutet et al., 2006; Goyal et al., 2016; Jayachandran et al., 2009; Rowe et al., 2011), we analyzed the expression of this transcription factor in the human fibrotic skin disease scleroderma (SSc). Quantitative PCR analysis of skin biopsies revealed an ∼5-fold increase in SNAI1 relative to that in normal skin biopsies (Figure 1a). Furthermore, we observed that the expression of the SNAI1 protein is localized in the nucleus of basal epidermal keratinocytes (KCs) in patients with SSc (Figure 1b), whereas it is undetectable in normal skin. We previously developed a transgenic (Tg) mouse with SNAI1 targeted to the basal layer of the epidermis (SNAI1 Tg) (Jamora et al., 2005) (Figure 1b) and that develops dermal fibrosis (Nakasaki et al., 2015; Pincha et al., 2018a). Interestingly, although the RNA of the SNAI1 transgene is expressed from neonatal to adulthood (Figure 1c), the protein is detected only neonatally (Figure 1d). Consequently, the transient expression of the SNAI1 protein in the epidermis is sufficient to initiate the program dermal fibrogenesis.

To test the extent to which the SNAI1 Tg mouse recapitulates the diagnostic characteristics of SSc, we benchmarked the phenotype against the clinical parameters as defined in the European League Against Rheumatism and the American College of Rheumatology 2013 criteria (Van Den Hoogen et al., 2013). The most dramatic gross phenotypes in the SNAI1 Tg mice at postnatal day 9 are puffy tails with necrotic ulcers, shiny skin (Figure 1e), and puffy paws with edema (Figure 1f). These features are similar to puffy fingers and necrotic lesions of digital ulcers observed in the tips of the fingers or toes in patients with SSc (Schiopu et al., 2010). One of the earliest signs of SSc is Raynaud's phenomenon, in which the blood vessels in the extremities contract upon exposure to cold stress, leading to the discoloration of the tissue (Wigley and Flavahan, 2016). A brief cold challenge was applied to the tail of mice on postnatal day 9 for 2 minutes and was observed by four independent viewers who were blinded to the genotype of the mice. The cold challenge led to blanching of the tissue in the Tg mouse that later recovered after 24 hours but had no discoloration effect in the wild type (WT) mice (Figure 1g).

One of the later hallmarks of the SSc is the development of autoantibodies against nuclear proteins (Takehara and Sato, 2005). Interestingly, the serum from SNAI1 Tg mice on postnatal day 60 contained antibodies against nuclear proteins (Figure 1h and Supplementary Table S1), although this observation was not consistently reproducible in the serum collected from mice on postnatal day 9. SSc is a progressive disease, in which fibrosis starts in the extremities but later involves internal organs. In line with this, we observed that SNAI1 Tg mouse on postnatal day 60 showed vascular leakage in the lung (Figure 1i), which is often an early sign of lung involvement in SSc (Bruni et al., 2018). However, we did not observe any evidence of lung fibrosis at this age (Supplementary Figure S1a). Another major organ involved in scleroderma is the heart (Champion, 2008), and cardiac abnormalities usually portend poorly for the patient. Echocardiography examination revealed that SNAI1 Tg mice aged 1 year present with cardiac hypertrophy. This is manifested as increases in heart size, left ventricle wall thickness, increased ejection fraction and fractional shortening, and decreased left ventricle volume at systole (Figure 1j and Supplementary Figure S1b). Furthermore, in later stages of dSSc skin, skin ulcers are commonly observed over the extensor surfaces of the body (Suliman et al., 2017). Consistent with this, the dorsal neck lesions first appear in mice on postnatal day 90 (Supplementary Figure S1c) and can be observed in Tg mice that are aged 1 year (Supplementary Figure S1d).

In summary, five of the European League Against Rheumatism and the American College of Rheumatology classification criteria for SSc were met in the SNAI1 Tg mice (Supplementary Table S2). Overall, the characterization of the SNAI1 Tg mice shows that transient expression of this transcription factor is sufficient to launch the development of fibrosis. Moreover, similar to the clinical sequelae of SSc, the fibrotic phenotypes are long lasting in the Tg mouse and eventually encompass the skin, connective tissue, and internal organs.

SNAI1 Tg mice recapitulate histological and molecular characteristics of SSc

At the histological level, skin from patients with SSc exhibits an early increase in dermal thickness and a later loss of dermal white adipose tissues (Marangoni et al., 2015). The dermal thickness of the SNAI1 Tg skin was significantly increased by ∼1.5-fold relative to that of WT as early as postnatal day 9 and increased to ∼3-fold at postnatal day 60 (Figure 2a and b). However, the loss of dermal white adipose tissues was significant only in Tg skin at postnatal day 60 (Figure 2a and b). We also observed an increase in the amount of collagen (Figure 2c and d) (Nakasaki et al., 2015) and fibronectin (Supplementary Figure S2a and b) in the dermis of neonatal mice that substantially increases as the mice age. In summary, these data suggest that fibrogenesis initiates neonatally and progresses until it is most pronounced in the adult skin.

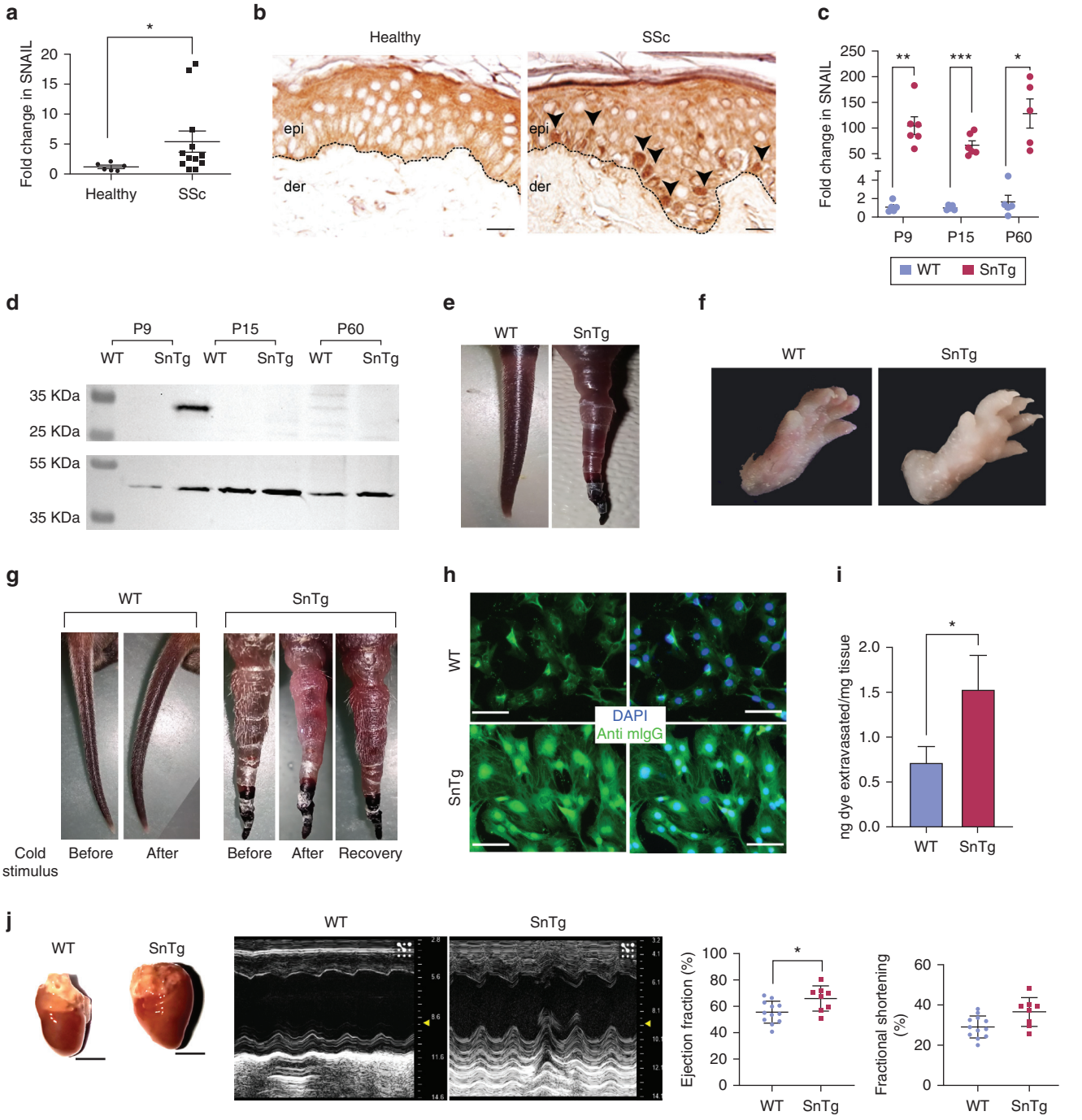

Figure 1. The SNAI1 Tg mouse recapitulates the diagnostic feature of scleroderma. (**a**) qPCR for expression of *SNAI1* gene in healthy skin (n = 6 patients) and skin from patients with SSc (n = 12 patients) and performed in three technical replicates. (**b**) Immunohistochemistry for SNAI1 protein in skin sections. The black dotted line denotes the basement membrane that separates the epi from the der. Arrows denote positively stained cells. Bar = 20 μm. (**c**) qPCR for SNAI1 expression in WT and SNAI1 Tg mice skin samples taken on P9 (WT, n = 5; SNAI1 Tg, n = 6), P15 (WT, n = 5; SNAI1 Tg, n = 6), and P60 (WT, n =5; SNAI1 Tg, n = 5). All samples were performed in three technical replicates for qPCR. (**d**) Western blot for SNAI1 using skin samples. (**e**) Gross appearance of tail. (**f**) Gross appearance of paws. (**g**) Cold challenge test for Raynaud's phenomenon. Images of the tail were taken before and after exposure to ice. Recovery was 24 hr after cold challenge. (**h**) Antinuclear antibody staining using serum collected from P60 mice. Bar = 100 μm (serum dilution 1:10). (**i**) Lungs of P60 mice were analyzed for vascular leakage using dye extravasation assay (WT, n =3 mice; SNAI1 Tg, n = 3 mice; three measurements per mouse). (**j**) Comparison of gross anatomy (left panel) and echocardiogram (middle panel) of the heart of WT and SNAI1 Tg mice aged 1 year. Bar = 5 cm. Comparison of values for ejection fraction and fractional shortening obtained from echocardiogram between WT (n = 12 mice) and SNAI1 Tg (n = 8 mice) mice (right panel). Error bars represent mean ± SEM. *P*-value was calculated using (**a**) Mann–Whitney *U* test and (**c, i, j**) Welch's *t*-test. $^{*}P < 0.05$, $^{**}P < 0.01$, and $^{***}P < 0.001$. der, dermis; epi, epidermis; hr, hour; P15, postnatal day 15; P60, postnatal day 60; P9, postnatal day 9; SnTg, SNAI1 transgenic; SSc, systemic sclerosis; Tg, transgenic; WT, wild type.

Given the early onset of this phenotype, we investigated the mechanisms underlying fibrogenesis in the SNAI1 Tg mouse, by analyzing the transcriptome of postnatal day 9 skin through RNA sequencing. A total of 353 genes were differentially expressed ($\log_2$ fold change > 1.5 for upregulated or ≤ 1.5 for downregulated, adjusted $P < 0.05$), and of these,

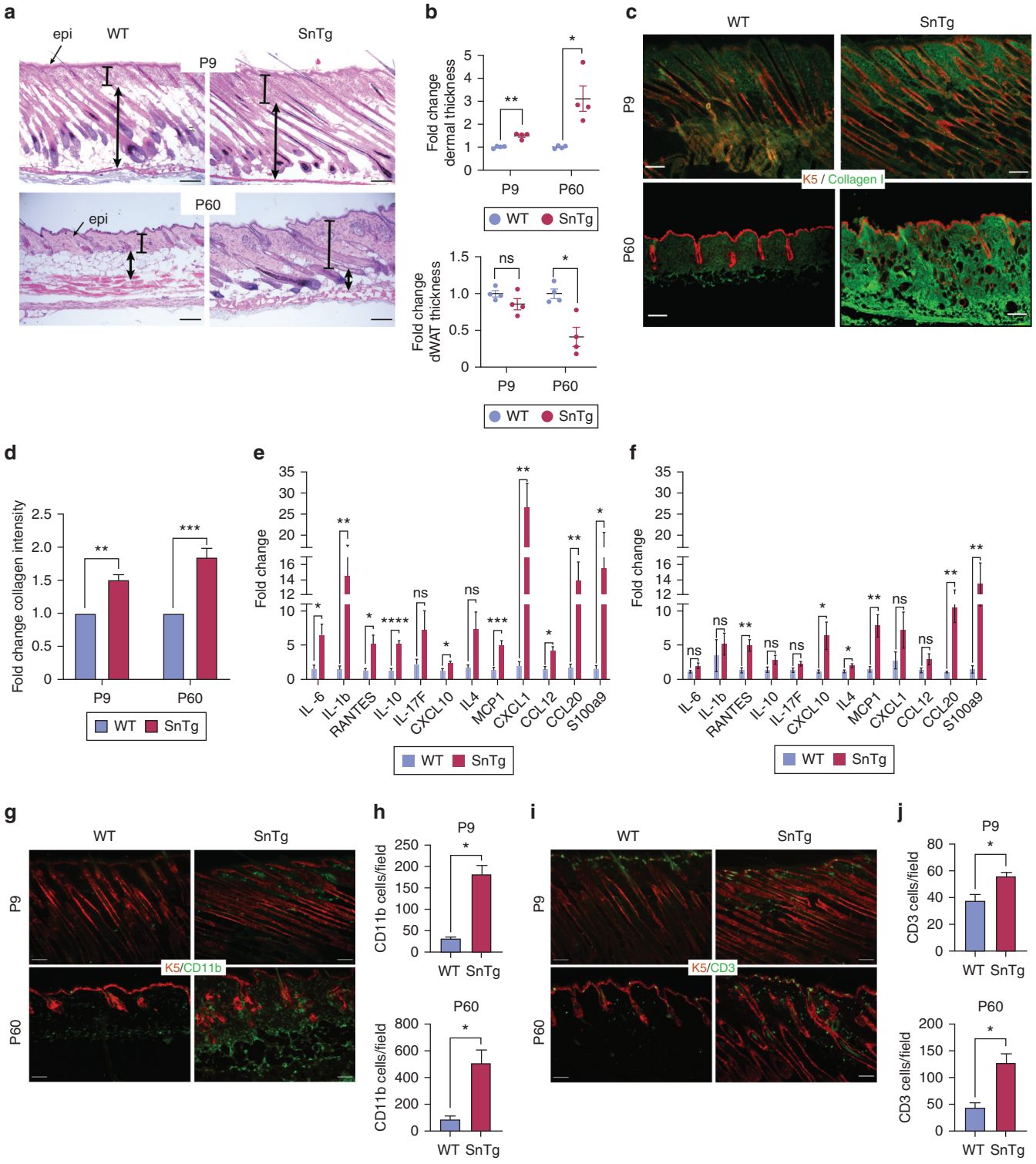

Figure 2. SNAI1 Tg mice recapitulate histological and molecular characteristics of SSc. (**a**) H&E staining of skin sections. Block lines denote dermal thickness, and lines with double-headed arrows denote dWAT thickness. Bar = 100 μm. (**b**) Quantification of dermal and dWAT thickness in P9 WT (n = 4) and SNAI1 Tg (n = 4) and P60 WT (n = 4) and SNAI1 Tg (n = 4) mice (each dot represents an individual mouse, two microscopic fields per mouse were analyzed). (**c**) Immunofluorescence of K5 (red) and collagen 1 (green). Bar = 100 μm. (**d**) Quantification of dermal collagen staining in P9 WT (n = 4 mice) and SNAI1 Tg (n = 4 mice) and P60 WT (n = 5 mice) and SNAI1 Tg (n = 5 mice) mice (two microscopic fields per mice were analyzed). (**e**) qPCR for inflammatory cytokines gene expression in WT (n = 8 mice) and SNAI1 Tg (n ≥ 6 mice) skin at P9 (three technical replicates per mouse were performed). (**f**) qPCR for inflammatory cytokines gene expression in WT (n = 9 mice) and SNAI1 Tg (n = 7 mice) skin at P60 (three technical replicates per mouse were performed). (**g**) Immunofluorescence of K5 (red) and CD11b (green). Bar = 100 μm. (**h**) Quantification of the number of $CD11b^+$ cells per microscopic field in P9 WT (n = 3 mice) and SNAI1 Tg (n = 3 mice) and P60 WT (n = 3 mice) and SNAI1 Tg (n = 3 mice) mice (two microscopic fields per mouse were counted). (**i**) Immunofluorescence of K5 (red) and CD3 (green). Bar = 100 μm. (**j**) Quantification of the number of $CD3^+$ cells per microscopic field in P9 WT (n = 3 mice) and SNAI1 Tg (n = 3 mice) and P60 WT (n = 3 mice) and SNAI1 Tg (n = 3 mice) mice (two microscopic fields per mouse were counted). The error bars represent mean ± SEM. *P*-value was calculated using

276 genes were upregulated, and 77 were downregulated (Supplementary Figure S2c and d). WEBGSALT (WEB-based Gene SeT AnaLysis Toolkit) analysis (Liao et al., 2019) revealed enrichment of Gene Ontology terms associated with an inflammatory response (Supplementary Figure S2e). Of the upregulated genes in the SNAI1 Tg mice with known human orthologs, 60 (35%) were also upregulated in patients with early dSSc (GSE130955 [Skaug et al., 2020]) (Supplementary Figure 2f) (2% overlap, representation factor = 3.1, $P <$ 9.495e-17). Given the early onset of fibrosis in the SNAI1 Tg mice, we compared the gene profile with that of pediatric patients with localized SSc (Mirizio et al., 2021) and found 14% orthologous genes overlapped (GSE166861 [Mirizio et al., 2021]) (Supplementary Figure S2f) (1.28% overlap, representation factor 2, $P <$ 7.724e-4). Interestingly, the overlapping genes were enriched in inflammatory genes (Supplementary Figure S2g and h). Moreover, genes from the RNA-sequencing data such as *CXCL1*, *CCL12*, *CCL20*, and *S100A9* were also elevated in SNAI1 Tg skin at postnatal days 9 and 60 (Figure 2e and f and Supplementary Table S3). In addition, inflammatory signals found in SSc such as IL-6, IL-10, IL-4, CXCL10, and monocyte chemotactic protein-1 (Crescioli et al., 2018; Fukayama et al., 2020; Hudson et al., 2005; Kawaguchi, 2017; Raja and Denton, 2015; Salmon-Ehr et al., 1996) were also upregulated (Figure 2e and f and Supplementary Table S3). In contrast, IL-17F did not show any significant upregulation. Consistent with the upregulation of inflammatory cytokine expression, we observed a marked increase in the number of $CD11b^+$ cells (such as monocytes, neutrophils, and macrophages) (Figure 2g and h), T cells (Figure 2i and j), and mast cells (Supplementary Figure S2i and j) in the SNAI1 Tg skin.

Secreted Mindin (SPON2) from SNAI1 Tg KCs mediates fibrogenesis

The central process in the establishment of dermal fibrosis is the activation of fibroblasts into myofibroblasts (Schuster et al., 2021) that are capable of secreting excessive amounts of extracellular matrix proteins and many inflammatory cytokines. Thus, the source of these activated fibroblasts has generated widespread interest. The canonical role of SNAI1 in mediating an epithelial–mesenchymal transition during embryogenesis is widely extrapolated to be a method to produce activated fibroblasts from neighboring SNAI1-expressing epithelial cells. Surprisingly, lineage tracing analysis revealed that none of the dermal fibroblasts in the Tg skin were a product of an epithelial–mesenchymal transition (Figure 3a). The β-galactosidase staining observed in the dermis was localized to sebaceous glands (Supplementary Figure S3a) owing to the hyperplasia that we have previously reported (Du et al., 2010). These data suggest a non–epithelial–mesenchymal transition function of SNAI1 to activate resident dermal fibroblasts through the exchange of signals between the epidermal and dermal compartments.

To test this hypothesis, we collected conditioned media (CM) from WT and SNAI1 Tg epidermal explants and assessed their sufficiency to activate primary dermal fibroblasts using a collagen contraction assay. Interestingly, SNAI1 Tg epidermal CM induced 1.7-fold higher activity than the WT CM (Supplementary Figure S3b). However, the epidermis is not a homogenous tissue of KCs but also contains other cell populations, including resident immune cells. To determine whether the Tg KCs are the source of the fibroblast-activating signal(s), we used CM from SNAI1 Tg primary KCs and found that it was sufficient to induce collagen contraction (Figure 3b) and significantly upregulated α-smooth muscle actin expression (Supplementary Figure S3c). Furthermore, primary dermal fibroblasts treated with SNAI1 Tg KCs CM resulted in a significant upregulation of CXCL1 and IL-6 but not of RANTES, IL-17F, and IL-4. However, CCL12, CCL20, and IL-1b were downregulated by SNAI1 Tg CM (Figure 3c and Supplementary Table S3). What then is the factor(s) in the SNAI1 Tg CM responsible for fibroblast activation? We have previously reported that Fibulin-5 and PAI-1 are secreted by SNAI1 Tg KCs that contribute to fibrosis by altering tissue stiffness (Nakasaki et al., 2015) and mast cell recruitment (Pincha et al., 2018a), respectively. However, we found that ablating these genes from SNAI1 Tg background only results in a partial reduction of the fibrotic phenotype. This incomplete abrogation of the fibrotic phenotype implies that other factors are involved in fibrogenesis, each contributing in an additive or synergistic manner. Thus, we have been systematically analyzing different proteins secreted by SNAI1 Tg KCs to understand their potential role(s) in mediating the fibrotic phenotype in the mouse model. Another protein secreted by SNAI1 Tg KCs is Mindin (Badarinath et al., 2022), an F-spondin family protein (also known as SPON2), which has previously been reported to be overexpressed in some solid tumors (Feng et al., 2019; Kang et al., 2020; Lu et al., 2020; Qian et al., 2012; Schmid et al., 2016; Yuan et al., 2017) and fibrotic conditions (Moon et al., 2009; Murakoshi et al., 2011a; Sun et al., 2015; Yang et al., 2020; Zhang et al., 2018). In pathological contexts, Mindin has been implicated in allergic (Tighe et al., 2011), inflammatory, and fibrotic diseases (Murakoshi et al., 2011a; Wang et al., 2013; Yang et al., 2020; Zhang et al., 2018), and over the years, it has emerged as a prognostic and diagnostic biomarker for multiple carcinomas (Feng et al., 2019; Liao et al., 2010; Lu et al., 2020; Parry et al., 2005; Schmid et al., 2016; Yuan et al., 2017; Zhang et al., 2015). Mindin has also been reported as a proinflammatory and profibrotic molecule in fibrotic conditions such as renal fibrosis (Yang et al., 2020), atherosclerosis (Zhang et al., 2018), Ehlers–Danlos syndromes (Chiarelli et al., 2019), and Reinke's edema (Grill et al., 2021) and cardiac remodeling post-myocardial infarction (Moon et al., 2009). It is a proposed biomarker for diabetic nephropathy (Murakoshi et al., 2011a), osteoarthritis (Balakrishnan et al., 2014), and prostate cancer (Qian et al., 2012). Mindin is also seemingly involved in response to injury. For instance, the urinary secretion of Mindin in diabetic nephropathy is a result of podocyte injury (Murakoshi et al., 2011b). Mindin has also

(**b, e, f, h, j**) two-tailed Welch's *t* test and (**d**) ratio-paired *t* test. *$P < 0.05$, **$P < 0.01$, ***$P < 0.001$, ****$P < 0.0001$; ns, $P > 0.05$. dWAT, dermal white adipose tissue; epi, epidermis; K5, keratin 5; ns, nonsignificant; P60, postnatal day 60; P9, postnatal day 9; SnTg, SNAI1 transgenic; SSc, systemic sclerosis; Tg, transgenic; WT, wild type.

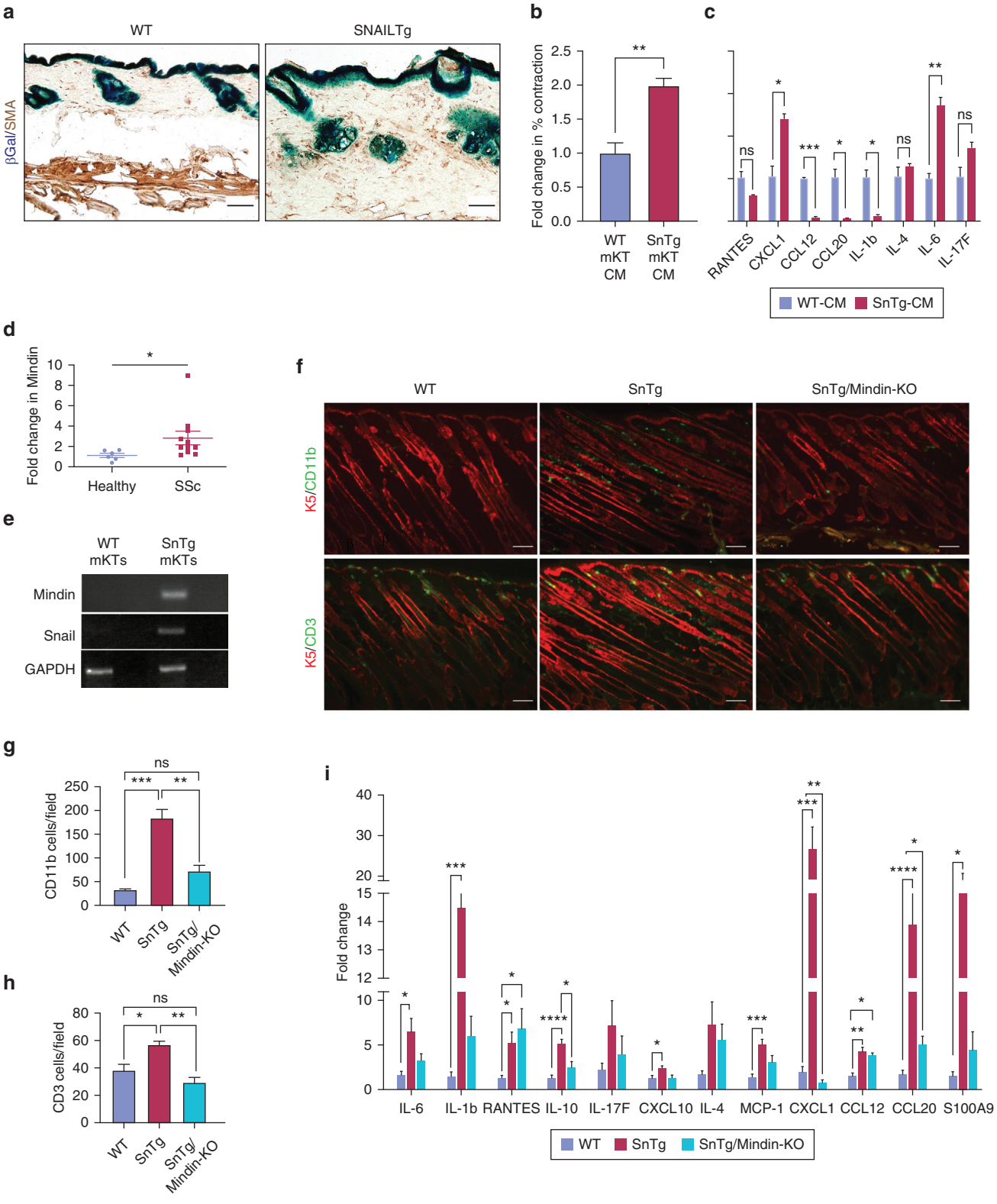

Figure 3. Secreted Mindin from SNAI1 Tg keratinocytes, not an EMT, causes the early fibrotic phenotype. (**a**) Lineage tracing of the WT and SNAI1 Tg mice using the K14-Cre R26R reporter (blue). Activated fibroblasts are stained with αSMA (brown). Bar = 50 μm. (**b**) Fibroblast activation was measured with the collagen contraction assay. CM from primary keratinocytes from WT (n = 5 biological replicates) and SNAI1 Tg (n = 3 biological replicates) mice. (**c**) qPCR for inflammatory cytokines gene expression in fibroblasts treated with WT (n = 3 biological replicates) and SNAI1 Tg (n = 3 biological replicates) keratinocytes CM performed in three technical replicates. (**d**) Expression of Mindin RNA in biopsies from healthy (n = 6 patients) and SSc (n = 12 patients) skin. Healthy and SSc skins are the same patient samples used for Figure 1a. (**e**) PCR for Mindin and SNAI1 in primary keratinocytes. GAPDH is used as a loading control. (**f**) Skin from P9 mice skin was stained for K5 (red) and either CD11b$^+$ cells (green) or T cells (CD3, green). Bar = 100 μm. (**g**) Quantification of the number of CD11b$^+$ cells per microscopic field in P9 WT (n = 3 mice), SNAI1 Tg (n = 3 mice), and SNAI1 Tg/Mindin-KO mice (n = 3 mice) (two microscopic fields per mouse were counted; WT and SNAI1 Tg data are same as in Figure 2h). (**h**) Quantification of the number of CD3$^+$ cells per microscopic field in P9 WT (n = 3 mice), SNAI1

been shown to activate NF-κB signaling in ischemic brain injury and regulate the production of inflammatory cytokines and infarct size (Wang et al., 2013).

Interestingly, we found that Mindin is overexpressed in the skin biopsies from patients with SSc (Figure 3d). Moreover, Mindin RNA is exclusively expressed by SNAI1 Tg but not WT epidermal KCs (Figure 3e). Because Mindin is known to impact macrophages (Jia et al., 2005; Li et al., 2020), T cells (Li et al., 2006), and proinflammatory signaling pathways (Guleng et al., 2010; Yang et al., 2020), we postulated that Mindin may be required for the inflammatory microenvironment of the SNAI1 Tg skin that is crucial for fibrogenesis. In this regard, we found that ablating Mindin expression in the SNAI1 Tg background resulted in a drastic reduction in the number of infiltrating T cells and $CD11b^+$ cells (such as monocytes, neutrophils, and macrophages) in postnatal day 9 skin (Figure 3f–h). However, there was no significant reduction in the number of mast cells in SNAI1 Tg/Mindin-knockout skin (Supplementary Figure S3d and e), which we have previously shown is regulated by PAI-1 (Pincha et al., 2018a).

As expected, inflammatory cytokine expression of IL-10, CXCL-1, and CCL-20, which was upregulated in the skin of the SNAI1 Tg mice on postnatal day 9, was reduced in SNAI1 Tg/Mindin-knockout mice (Figure 3i and Supplementary Table S3). Interestingly, the reduction in T cells and $CD11b^+$ cells (Supplementary Figure S3f–i) and inflammatory cytokines (Supplementary Figure S3j) was only apparent in postnatal day 9 but not in postnatal day 60 skin. By postnatal day 60, other inflammatory signals in the SNAI1 Tg skin may override the early protection provided by removing Mindin in the Tg background.

Mindin stimulates proinflammatory cytokines in fibroblasts that drive fibrogenesis

We postulated that because Mindin is secreted from SNAI1 Tg KCs, it may need a relay system to recruit immune cells from circulation. One link between the epidermis and vasculature may be the activated fibroblasts, which have emerged as an important signaling node for coordinating various processes associated with fibrogenesis (Davidson et al., 2021). In particular, myofibroblasts secrete a number of inflammatory cytokines and chemokines.

To examine the potential effect of Mindin on fibroblasts, we treated primary dermal fibroblasts with recombinant Mindin and performed an RNA-sequencing analysis. We found that 1,232 genes were upregulated and that 1,274 genes were downregulated (adjusted $P < 0.001$, $\log_2$ fold change > 0.5, or $\log_2$ fold change ≤ 0.5). Interestingly, we found that the majority of Gene Ontology terms enriched for the upregulated genes are related to inflammatory processes (Supplementary Figure S4a) and, in particular, are involved in macrophage and T-cell migration and recruitment (Supplementary Figure S4b). Thus, although Mindin is known to directly aid in the recruitment of macrophages (Jia et al., 2005), it may also act on fibroblasts to increase the levels of cytokine expression that can amplify the signal for the migration and homing of immune cells into the skin. In line with this, we found a significant overlap of 16 genes in Mindin-treated fibroblasts and in SNAI1 Tg mouse skin (Supplementary Figure S4c) (representation factor = 1.9, $P < 0.009$), which were enriched for inflammatory processes (Supplementary Figure S4d). Similarly, there is a significant overlap of 182 upregulated genes between patients with early dSSc and Mindin-treated fibroblasts (Supplementary Figure S4e and f) and an overlap of 44 genes with pediatric patients with localized SSc (Supplementary Figure S4g and h). Many genes such as *Rantes*, *Cxcl1*, *Il6*, *Il1b*, *Ccl12*, and *Ccl20* that we found to be upregulated in the SNAI1 Tg skin were confirmed by qPCR analysis of primary dermal fibroblasts treated with Mindin (Figure 4a and Supplementary Table S3). However, not all inflammatory cytokines found in the SNAI1 skin can be recapitulated by Mindin-treated fibroblasts. For instance, IL-6, IL-17F, and IL-4 showed no change or were downregulated.

We then assessed the dependence of the SNAI1 Tg phenotype on Mindin. In neonatal skin, we observed that the heightened dermal thickness in the SNAI1 Tg skin was reduced to WT levels on ablation of Mindin (Figure 4b and c). Even in adult skin (postnatal day 60), the 3.2-fold increase in dermal thickness in the SNAI1 Tg skin was substantially reduced, although it remained slightly higher than WT levels. Remarkably, the loss of dermal white adipose tissue seen in the adult Tg skin is reversed on deletion of Mindin in the SNAI1 background. Likewise, the levels of dermal collagen were reduced during deletion of Mindin in the SNAI1 background in both neonatal and adult mice (Figure 4d and e). In addition, many of the symptoms associated with scleroderma that are recapitulated in the SNAI1 Tg mouse are substantially reduced when Mindin is removed from the Tg background (Supplementary Table S2). Altogether these data reveal that Mindin plays a critical role in SNAI1-mediated fibrogenesis because the absence of this matricellular protein largely attenuates the fibrotic phenotype.

DISCUSSION

We report a mouse model on the basis of the Tg overexpression of SNAI1 in the basal epidermal KCs to mimic its expression in the SSc skin (Figure 4f). Of the seven criteria of the 2013 American College of Rheumatology/European League Against Rheumatism (Van Den Hoogen et al., 2013), the SNAI1 Tg mouse matched at least five: puffy fingers; Raynaud's phenomenon; necrotic tip ulcers; the presence of antinuclear antibodies; and thickening of the skin, especially in the paws and tail. Although the leather-like appearance

Tg (n = 3 mice), and SNAI1 Tg/Mindin-KO (n = 3) mice (two microscopic fields per mouse were counted; WT and SNAI1 Tg data are same as in Figure 2j). (**i**) qPCR for inflammatory cytokines gene expression in WT (n = 8 mice), SNAI1 Tg (n ≥ 6 mice), and SNAI1 Tg/Mindin-KO (n = 3 mice) skin at P9 (three technical replicates per mice were performed; WT and SNAI1 Tg data are same as in Figure 2e). The error bars represent mean ± SEM. *P*-value was calculated using (**b, c**) two-tailed Welch's *t* test, (**d**) Mann–Whitney *U* test, and (**g–i**) one-way ANOVA followed Tukey's post hoc analysis. *$P < 0.05$, **$P < 0.01$, ***$P < 0.001$, and ****$P < 0.0001$. αSMA, α-smooth muscle actin; β-Gal, β-galactosidase; CM, conditioned media; EMT, epithelial–mesenchymal transition; K5, keratin 5; KO, knockout; MCP-1, monocyte chemotactic protein-1; ns, nonsignificant; P9, postnatal day 9; SnTg, SNAI1 transgenic; SSc, systemic sclerosis; Tg, transgenic; WT, wild type.

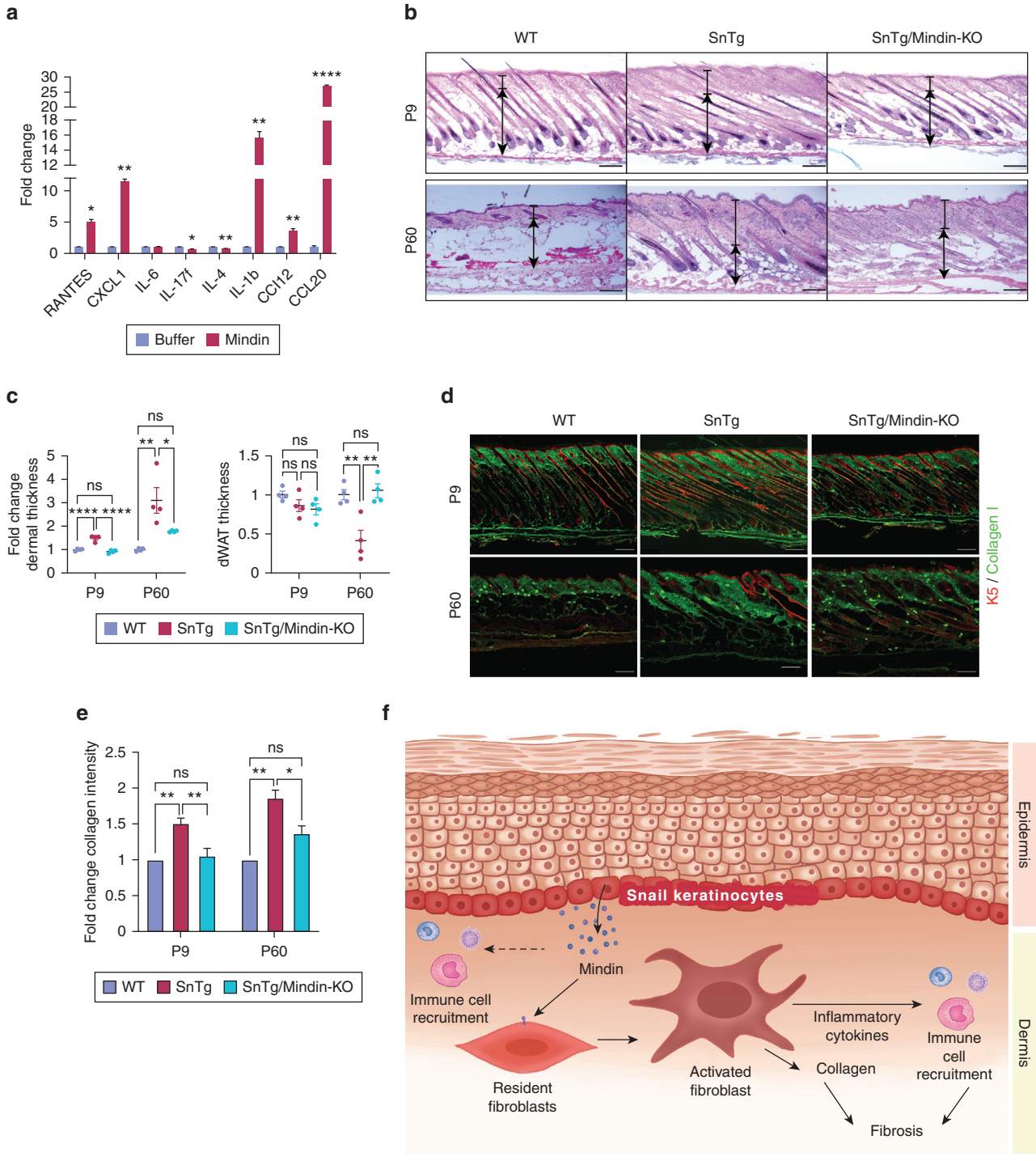

Figure 4. Mindin mediates the proinflammatory activation of fibroblasts and aids in fibrogenesis. (**a**) qPCR for inflammatory cytokine expression in fibroblasts treated with buffer control (n = 3 technical replicates) or Mindin (n = 3 technical replicates). Quantification is representative of three biological replicates. (**b**) H&E staining for WT, SNAI1 Tg, and SNAI1 Tg/Mindin-KO skin sections taken at P9 or P60. Blocked lines denote dermal thickness, and lines with arrowheads denote dWAT thickness. Bar = 100 μm. (**c**) Quantification of H&E-stained sections for dermal thickness and dWAT in WT (n = 4 mice), SNAI1 Tg (n = 4 mice), and SNAI1 Tg/Mindin-KO (n = 4 mice) mice (data for WT and SNAI1 Tg are the same as those used in Figure 2b). (**d**) Immunofluorescence for K5 (red) and collagen (green) in WT, SNAI1 Tg, and SNAI1 Tg/Mindin-KO skin. Bar = 100 μm. (**e**) Quantification of dermal collagen staining in P9 WT (n = 4 mice) and SNAI1 Tg (n = 4 mice), SNAI1 Tg/Mindin-KO (n = 4 mice) and P60 WT (n = 5 mice), SNAI1 Tg (n = 5 mice), and SNAI1 Tg/Mindin-KO (n = 5 mice) mice (two microscopic fields per mice were analyzed; data for WT and SNAI1 Tg are the same as in Figure 2d). (**f**) Model of SNAI1-mediated fibrosis with Mindin involved in fibroblast activation. Error bars represent mean ± SEM. *P*-value was calculated using (**a**) two-tailed Welch's *t* test and (**c, e**) one-way ANOVA followed by Tukey's posthoc analysis. **P* < 0.05, ***P* < 0.01, ****P* < 0.001, *****P* < 0.0001. dWAT, dermal white adipose tissue; K5, keratin 5; KO, knockout; P60, postnatal day 60; P9, postnatal day 9; SnTg, SNAI1 transgenic; Tg, transgenic; WT, wild type.

(lesion) of the skin on the paws and tail was apparent, it is difficult to clearly score sclerodactyly owing to the natural curling of the murine paws. Similarly, red spots and sores were observed in the paws and limbs of SNAI1 Tg mice and, in later stages, on lesions around the dorsal neck area. However, whether they represent telangiectasia will require further evaluation.

The robust inflammatory phenotype in the SNAI1 Tg mouse begs the question of how the expression of SNAI1 in epidermal KCs leads to the dermal infiltration of immune cells. Interestingly, the function of SNAI1 in our mouse model of cutaneous fibrosis is epithelial–mesenchymal transition independent and relies on signaling proteins such as Mindin. Although Mindin is well-known as a matricellular protein (Jia et al., 2005), it can also participate in cell signaling pathways such as a pathogen-associated molecular pattern to directly recruit macrophages (He et al., 2004). In this study, we present evidence that Mindin can activate primary dermal fibroblasts leading to the expression of inflammatory cytokines and chemokines that can recruit both adaptive and innate immune cells to the skin. This observation is consistent with a previous finding that Mindin can activate proinflammatory signaling through the NFκB pathway in HK-2 cells (Guleng et al., 2010; Wang et al., 2013; Yang et al., 2020). Furthermore, we found that Mindin is essential for the early inflammatory response in the SNAI1 Tg mouse. Crippling this cutaneous inflammation through the genetic knockout of Mindin completely abrogated the dermal fibrosis in the neonatal (postnatal day 9) SNAI1 Tg mouse. That said, the temporal analysis of the SNAI1 Tg phenotype has revealed an intriguing aspect of fibrosis. In contrast to the neonatal SNAI1 Tg mouse, as the mouse reached adulthood, the absence of Mindin in the postnatal day 60 mouse did not sustain the reduction of cutaneous inflammation. Nevertheless, there was still a substantial decrease in dermal thickness in the absence of Mindin in the adult SNAI1 Tg mouse, albeit not to levels comparable with that in WT skin. Consistent with this was our observation that Mindin can increase collagen expression in dermal fibroblasts (Kataria et al., 2022[1]). Together, these observations suggest that inflammation is more important at the initial stages of fibrogenesis rather than at the later stages of the pathogenesis or in the maintenance of this pathology. This is consistent with the model that inflammation is an early driver of scleroderma, whereas the later stages of the disease are marked by fibroproliferation (Milano et al., 2008; Skaug et al., 2020). In addition, the transient effect of Mindin on inflammation despite its effective suppression of fibrosis suggests that this matricellular protein likely has other important roles such as regulating the activity of myofibroblasts.

Altogether the data suggest that specific targeting of SNAI1 and/or Mindin has the potential to fill the gap in effective therapeutic targets to halt the progression of SSc. In line with this, Mindin is also upregulated in other mouse models of SSc (Supplementary Figure S5). Moreover, Mindin has also been reported as a proinflammatory and profibrotic molecule in other conditions (Chiarelli et al., 2019; Grill et al., 2021; Moon et al., 2009; Yang et al., 2020; Zhang et al., 2018). A note of caution is worthwhile because all fibrotic tissues may not be completely the same, and the role of Mindin may not be universal in all tissues as a profibrotic factor. For instance, Mindin has been implicated to be antifibrotic in liver steatosis (Zhu et al., 2014) and possibly in cardiac hypertrophy (Bian et al., 2012).

[1] Kataria S, Rana I, Badarinath K, Zaarour RF, Kansagara G, Zirmire RK, et al. Mindin differentially regulates fibroblast subpopulations via distinct members of the Src family kinases during fibrogenesis. bioRxiv 2022.

MATERIALS AND METHODS

Animal studies

C57Bl6 (WT) mice were obtained from The Jackson Laboratory (Bar Harbor, Maine), Mindin-knockout mice were obtained from You-Wen He (Duke University, Durham, NC), and the SNAI1 Tg mouse was described earlier (Jamora et al., 2005).

Gene expression

RNA extraction and PCR analysis were as previously described (Pincha et al., 2018a). Primer sequences are presented in Supplementary Table S4.

Human SSc skin

Analysis of human skin was as previously described (Nakasaki et al., 2015). Characteristics of patients' samples are provided in Supplementary Table S5. Human skin samples were acquired following written, informed consent by the donors.

Transcriptome data analysis

The differential gene expression analysis was performed using the CLC genomics workbench differential expression analysis tool (Gallardo-Escárate et al., 2014). The functional and pathway enrichments of the Gene Ontology terms and Kyoto encyclopedia of genes and genomes pathways (Kanehisa and Goto, 2000) associated with the differentially expressed transcripts were analyzed through WebGestalt tool (Liao et al., 2019). The *P*-values were corrected by Benjamini and Hochberg false discovery rate correction method, and the false discovery rate < 0.05 was considered statistically significant (Benjamini and Hochberg, 1995). Differentially expressed genes in the skin of human early dSSc were derived from GSE130955 (Skaug et al., 2020), and those of the skin of pediatric patients with localized scleroderma were from GSE166861 (Mirizio et al., 2021). Venn diagrams were obtained using Venny 2.1 (Oliveros, 2007). Representation factor and *P*-value were calculated using exact hypergeometric probability using the program (http://nemates.org/MA/progs/representation.stats.html).

Mindin expression in fibrotic mouse models

We searched gene expression omnibus microarray datasets for different mouse models from GSE61728 (Long et al., 2015), GSE71999 (Sargent et al., 2016), GSE17914 (Greenblatt et al., 2012), GSE97546 (Lv and Liu, 2017), GSE77326 (LeBleu, 2020), GSE200425 (Biasin et al., 2022), GSE31950 (Wang et al., 2012), GSE10849 (Augustus et al., 2008), GSE36496 (Wu and Brooks, 2012), GSE200409 (Chiba and Matsumoto, 2022).

Western blot

Western blotting was performed as previously reported (Pincha et al., 2018a). Antibodies used were hemagglutinin (1:1,000, ab 9110, Abcam, Cambridge, United Kingdom) and β-actin (1:4,000, A2228, Sigma-Aldrich, St. Louis, MO). The horseradish peroxidase–labeled secondary antibodies (Jackson ImmunoResearch Laboratories, West Grove, PA) were used at 1:5,000. Blots were developed on an ImageQuant LAS4000.

Histology and immunohistochemistry

Skin tissues were analyzed as previously reported (Pincha et al., 2018a) using the following antibodies at 1:200: keratin 5, collagen 1 (ab21286, Abcam), CD11b (ab8878, Abcam), CD3 (14-0041-85, eBiosciences, San Diego, CA), fibronectin (ab2413, Abcam), or serum. Secondary antibodies (Jackson ImmunoResearch Laboratories) were used at 1:300. Images were captured with an Olympus IX73 microscope or FV1000 confocal microscope and analyzed with Fiji software.

For quantification of dermal thickness, multiple measurements were made along the length of the H&E-stained sections perpendicular to the epidermis. The collagen and fibronectin staining was quantified by measuring the integrated density of staining in the dermis.

Raynaud's assay

Postnatal day 9 (neonatal) mice tails were kept on ice for approximately 2 minutes. The color change assessment was made by four independent observers while performing the cold challenge test, and images were captured with a camera immediately after the cold exposure and again after 24 hours.

Vascular leakage

Leakage of Evans Blue dye was performed as in the study by Wick et al. (2018).

Echocardiography

Cardiac function in WT and SNAI1 Tg mice at age 1 year was performed and analyzed as previously reported (Dhandapany et al., 2021).

Lineage tracing

K14-Cre R26R were crossed with K14-SNAI1 Tg mice to generate K14-Cre R26R/K14-SNAI1 Tg, and skin sections were probed for expression of β-galactosidase and α-smooth muscle actin using immunohistochemistry.

Cell culture

Primary dermal fibroblasts and epidermal KCs were isolated and cultured as described earlier (Nakasaki et al., 2015; Nowak and Fuchs, 2009). To collect CM WT and SNAI1 Tg, KCs were seeded in a 10-cm dish in low calcium E-media as described previously (Bhatt et al., 2022). On reaching confluency, low calcium E-media was replaced with serum-free low calcium E-media. CM was generated from confluent plates of WT and SNAI1 Tg KCs incubated for 16 hours in serum-free media. Primary fibroblasts were seeded in a 3.5 cm dish (150,000 cells/dish), and on reaching 80% confluency, they were treated with CM (1:1 ratio of CM and DMEM) from WT or SNAI1 Tg KCs for 16 hours. For accessing the effect of Mindin on fibroblasts, the primary fibroblasts seeded in a 3.5 cm dish (150,000 cells/dish) were treated with either buffer or Mindin (∼200 ng/ml) for 16 hours.

Mindin purification

Histidine-tagged Mindin was purified from CM collected from Chinese hamster ovary−Mindin cells using Ni-NTA beads (Thermo Fisher Scientific, Waltham, MA) according to the manufacturer's instructions.

Collagen contraction assay

Collagen contraction assay using rat tail collagen plugs (08-115, 1 mg/ml, MilliporeSigma, Burlington, MA) was previously reported (Pincha et al., 2018b).

Statistics

Comparisons of the two groups were done using a two-tailed Welch's *t* test or Mann−Whitney *U* test. Paired data were analyzed using ratio-paired *t* test. One-way ANOVA followed by Tukey's posthoc analysis was used for multiple-group comparisons. GraphPad Prism 6 (GraphPad Software, San Diego, CA) was used for all statistical analyses. Data represent the mean ± SEM. $P < 0.05$ were considered significant.

Study approval

Animal work was approved by the inStem Institutional Animal Ethics Committee following the norms specified by the Committee for the Purpose of Control and Supervision of Experiments on Animals (Government of India). Acquisition and processing of the human tissue were conducted according to the protocol approved by the Institutional Review Board of the Christian Medical College Vellore (Vellore, India). Informed consent was obtained from all patients for skin sample collection and experimentation. All experimental work was approved by the Institutional Biosafety Committee and the Institutional Human Ethics Committee of inStem.

Data availability statement

Datasets related to this article can be found at https://www.ncbi.nlm.nih.gov/bioproject/PRJNA846577/, hosted at Sequence Read Archive at the National Center for Biotechnology Information with Bioproject identification PRJNA846577.

ORCIDs

Isha Rana: http://orcid.org/0000-0002-1512-0000
Sunny Kataria: http://orcid.org/0000-0002-0690-6300
Tuan Lin Tan: http://orcid.org/0000-0001-5884-6808
Edries Yousaf Hajam: http://orcid.org/0000-0002-3589-5823
Deepak Kumar Kashyap: http://orcid.org/0000-0001-5352-0040
Dyuti Saha: http://orcid.org/0000-0002-5468-4853
Johan Ajnabi: http://orcid.org/0000-0002-9437-9300
Sayan Paul: http://orcid.org/0000-0001-6620-950X
Shashank Jayappa: http://orcid.org/0000-0002-6751-8344
Akhil S.H.P. Ananthan: http://orcid.org/0000-0002-2238-1006
Pankaj Kumar: http://orcid.org/0000-0002-8411-1634
Rania F. Zaarour: http://orcid.org/0000-0001-9132-5940
Haarshaadri J.: http://orcid.org/0000-0003-0089-3147
Gaurav Kansagara: http://orcid.org/0000-0003-0779-3165
Abrar Rizvi: http://orcid.org/0000-0003-2867-5758
Ravindra K. Zirmire: http://orcid.org/0000-0002-6003-2771
Krithika Badarinath: http://orcid.org/0000-0003-0941-5504
Sneha Uday Khedkar: http://orcid.org/0000-0001-5059-989X
Yogesh Chandra: http://orcid.org/0000-0002-9697-2909
Rekha Samuel: http://orcid.org/0000-0002-7405-4867
Renu George: http://orcid.org/0000-0003-4786-479X
Debashish Danda: http://orcid.org/0000-0002-2121-0942
Paul Mazhuvanchary Jacob: http://orcid.org/0000-0002-8780-3812
Rakesh Dey: http://orcid.org/0000-0002-8258-2969
Perundurai S. Dhandapany: http://orcid.org/0000-0001-7831-9570
You-Wen He: http://orcid.org/0000-0002-8983-2684
John Varga: http://orcid.org/0000-0001-8400-687X
Shyni Varghese: http://orcid.org/0000-0002-0004-7947
Colin Jamora: http://orcid.org/0000-0003-2127-2972

CONFLICT OF INTEREST

The authors state no conflict of interest.

ACKNOWLEDGMENTS

The authors would like to thank the members of Jamora laboratory for their critical review of the work and insightful discussions; Binita Dam, Syed Shahid Musvi, and Akshay Hegde for their technical assistance; and Ritoparna Hazra for designing the graphical model. This work was supported by core funds from inStem and grants from the Department of Biotechnology of the Government of India (BT/PR8738/AGR/36/770/2013 and BT/PR32539/BRB/10/1814/2019), the National Institutes of Health/National Institute of Arthritis and Musculoskeletal and Skin Diseases (5R01AR053185-03), and the American Cancer Society (15457-RSG-08-164-01-DDC) to CJ. PSD is supported by

the Department of Biotechnology/Wellcome Trust-Indian Alliance (IA/I/16/1/502367). IR and EYH were supported by the funding of the Indian Council of Medical Research (Senior Research Fellowship), and SK was partially supported by the National Centre for Biological Sciences. Animal studies were partially supported by the National Mouse Research Resource grant BT/PR5981/MED/31/181/2012;2013-2016;2018 and 102/IFD/SAN/5003/2017-2018 from the Department of Biotechnology. We thank the staff of the Bangalore Life Science Cluster Animal Care and Resource Centre and the Bangalore Life Science Cluster Central Imaging and Flow Cytometry Facility for technical assistance. This work was conducted in Bangalore, India.

AUTHOR CONTRIBUTIONS

Conceptualization: CJ, SK, IR, TLT; Data Curation: IR, SK, TLT; Formal Analysis: SK, TLT, DKK, DS, PK, RD, SP, SJ, GK, AR, RKZ, SUK, PSD; Funding Acquisition: CJ; Investigation: IR, SK, TLT, EYH, DKK, DS, JA, ASHPA, RFZ, HJ, GK, KB, SUK, YC; Methodology: CJ, SK, IR, TLT; Project Administration: IR, SK, TLT, CJ, SV; Resources: RS, RG, DD, PMJ, PSD, YWH, JV, CJ, SV; Software: PK, RD, SP, SJ, SK; Supervision: CJ, SV, JV, PSD; Validation: IR, SK, TLT, EYH, DKK, DS, JA, ASHPA, RFZ, HJ, GK, AR, RKZ, SUK, YC; Visualization: SK; Writing - Original Draft Preparation: SK, IR, TLT, CJ; Writing - Review and Editing: SK, CJ, JV

SUPPLEMENTARY MATERIAL

Supplementary material is linked to the online version of the paper at www.jidonline.org, and at https://doi.org/10.1016/j.jid.2022.10.011.

REFERENCES

Augustus AS, Buchanan J, Gutman E, Rengo G, Pestell RG, Fortina P, et al. Hearts lacking caveolin-1 develop hypertrophy with normal cardiac substrate metabolism. Cell Cycle 2008;7:2509–18.

Badarinath K, Dam B, Kataria S, Zirmire RK, Dey R, Kansagara G, et al. Snail maintains the stem/progenitor state of skin epithelial cells and carcinomas through the autocrine effect of matricellular protein Mindin. Cell Rep 2022;40:111390.

Balakrishnan L, Nirujogi RS, Ahmad S, Bhattacharjee M, Manda SS, Renuse S, et al. Proteomic analysis of human osteoarthritis synovial fluid. Clin Proteomics 2014;11:6.

Benjamini Y, Hochberg Y. Controlling the false discovery rate: a practical and powerful approach to multiple testing. J R Stat Soc B 1995;57:289–300.

Bhatt T, Dey R, Hegde A, Ketkar AA, Pulianmackal AJ, Deb AP, et al. Initiation of wound healing is regulated by the convergence of mechanical and epigenetic cues. PLoS Biol 2022;20:e3001777.

Bian ZY, Wei X, Deng S, Tang QZ, Feng J, Zhang Y, et al. Disruption of mindin exacerbates cardiac hypertrophy and fibrosis. J Mol Med (Berl) 2012;90:895–910.

Boutet A, De Frutos CA, Maxwell PH, Mayol MJ, Romero J, Nieto MA. Snail activation disrupts tissue homeostasis and induces fibrosis in the adult kidney. EMBO J 2006;25:5603–13.

Bruni C, Frech T, Manetti M, Rossi FW, Furst DE, De Paulis A, et al. Vascular leaking, a pivotal and early pathogenetic event in systemic sclerosis: should the door be closed? Front Immunol 2018;9:2045.

Champion HC. The heart in scleroderma. Rheum Dis Clin North Am 2008;34.181–viii.

Chiarelli N, Ritelli M, Zoppi N, Colombi M. Cellular and molecular mechanisms in the pathogenesis of classical, vascular, and hypermobile Ehlers–Danlos syndromes. Genes (Basel) 2019;10:609.

Crescioli C, Corinaldesi C, Riccieri V, Raparelli V, Vasile M, Del Galdo F, et al. Association of circulating CXCL10 and CXCL11 with systemic sclerosis. Ann Rheum Dis 2018;77:1845–6.

Davidson S, Coles M, Thomas T, Kollias G, Ludewig B, Turley S, et al. Fibroblasts as immune regulators in infection, inflammation and cancer. Nat Rev Immunol 2021;21:704–17.

Denton CP, Khanna D. Systemic sclerosis. Lancet 2017;390:1685–99.

Dhandapany PS, Kang S, Kashyap DK, Rajagopal R, Sundaresan NR, Singh R, et al. Adiponectin receptor 1 variants contribute to hypertrophic cardiomyopathy that can be reversed by rapamycin. Sci Adv 2021;7:eabb3991.

Du F, Nakamura Y, Tan TL, Lee P, Lee R, Yu B, et al. Expression of Snail in epidermal keratinocytes promotes cutaneous inflammation and hyperplasia conducive to tumor formation. Cancer Res 2010;70:10080–9.

Enzerink A, Vaheri A. Fibroblast activation in vascular inflammation. J Thromb Haemost 2011;9:619–26.

Feng Y, Hu Y, Mao Q, Guo Y, Liu Y, Xue W, et al. Upregulation of Spondin-2 protein expression correlates with poor prognosis in hepatocellular carcinoma. J Int Med Res 2019;47:569–79.

Fukayama M, Yoshizaki A, Fukasawa T, Ebata S, Kuzumi A, Yoshizaki-Ogawa A, et al. Interleukin (IL)-17F and IL-17E are related to fibrosis and vasculopathy in systemic sclerosis. J Dermatol 2020;47:1287–92.

Gallardo-Escárate C, Valenzuela-Muñoz V, Nuñez-Acuña G. RNA-Seq Analysis Using de novo transcriptome Assembly as a Reference for the salmon Louse Caligus rogercresseyi. PLoS One 2014;9:e92239.

Goyal A, Linskey KR, Kay J, Duncan LM, Nazarian RM. Differential expression of hedgehog and Snail in cutaneous fibrosing disorders: implications for targeted inhibition. Am J Clin Pathol 2016;146:709–17.

Greenblatt MB, Sargent JL, Farina G, Tsang K, Lafyatis R, Glimcher LH, et al. Interspecies comparison of human and murine scleroderma reveals IL-13 and CCL2 as disease subset-specific targets. Am J Pathol 2012;180:1080–94.

Grill M, Lazzeri I, Kirsch A, Steurer N, Grossmann T, Karbiener M, et al. Vocal fold fibroblasts in Reinke's edema show alterations involved in extracellular matrix production, cytokine response and cell cycle control. Biomedicines 2021;7(9):735.

Guleng B, Lian YM, Ren JL. Mindin is upregulated during colitis and may activate NF-kappaB in a TLR-9 mediated manner. World J Gastroenterol 2010;16:1070–5.

He YW, Li H, Zhang J, Hsu CL, Lin E, Zhang N, et al. The extracellular matrix protein mindin is a pattern-recognition molecule for microbial pathogens. Nat Immunol 2004;5:88–97.

Hudson LL, Rocca KM, Kuwana M, Pandey JP. Interleukin-10 genotypes are associated with systemic sclerosis and influence disease-associated autoimmune responses. Genes Immun 2005;6:274–8.

Jamora C, Lee P, Kocieniewski P, Azhar M, Hosokawa R, Chai Y, et al. A signaling pathway involving TGF-β2 and Snail in hair follicle morphogenesis. PLoS Biol 2005;3:e11.

Jayachandran A, Königshoff M, Yu H, Rupniewska E, Hecker M, Klepetko W, et al. SNAI transcription factors mediate epithelial–mesenchymal transition in lung fibrosis. Thorax 2009;64:1053–61.

Jia W, Li H, He YW. The extracellular matrix protein mindin serves as an integrin ligand and is critical for inflammatory cell recruitment. Blood 2005;106:3854–9.

Kanehisa M, KEGG GS. KEGG: Kyoto encyclopedia of genes and genomes. Nucleic Acids Res 2000;28:27–30.

Kang HG, Kim WJ, Noh MG, Chun KH, Kim SJ. SPON2 is upregulated through notch signaling pathway and promotes tumor progression in gastric cancer. Cancers (Basel) 2020;12:1439.

Kataria S, Rana I, Badarinath K, Zaarour RF, Kansagara G, Zirmire RK, et al. Mindin differentially regulates fibroblast subpopulations via distinct members of the Src family kinases during fibrogenesis. bioRxiv 2022.

Kawaguchi Y. Contribution of interleukin-6 to the pathogenesis of systemic sclerosis. SAGE 2017;2:S6–12.

Li H, Oliver T, Jia W, He YW. Efficient dendritic cell priming of T lymphocytes depends on the extracellular matrix protein mindin. EMBO J 2006;25:4097–107.

Li N, Liu S, Zhang Y, Yu L, Hu Y, Wu T, et al. Transcriptional activation of matricellular protein Spondin2 (SPON2) by BRG1 in vascular endothelial cells promotes macrophage chemotaxis [published correction appears in Front Cell Dev Biol 2021;9:657085] Front Cell Dev Biol 2020;8:794.

Liao CH, Yeh SC, Huang YH, Chen RN, Tsai MM, Chen WJ, et al. Positive regulation of spondin 2 by thyroid hormone is associated with cell migration and invasion. Endocr Relat Cancer 2010;17:99–111.

Liao Y, Wang J, Jaehnig EJ, Shi Z, Zhang B. WebGestalt 2019: gene set analysis toolkit with revamped UIs and APIs. Nucleic Acids Res 2019;47:W199–205.

Long KB, Li Z, Burgwin CM, Choe SG, Martyanov V, Sassi-Gaha S, et al. The Tsk2/+ mouse fibrotic phenotype is due to a gain-of-function mutation in the PIIINP segment of the Col3a1 gene. J Invest Dermatol 2015;135:718–27.

Lu H, Feng Y, Hu Y, Guo Y, Liu Y, Mao Q, et al. Spondin 2 promotes the proliferation, migration and invasion of gastric cancer cells. J Cell Mol Med 2020;24:98–113.

Marangoni RG, Korman BD, Wei J, Wood TA, Graham LV, Whitfield ML, et al. Myofibroblasts in murine cutaneous fibrosis originate from adiponectin-positive intradermal progenitors. Arthritis Rheumatol 2015;67:1062–73.

Milano A, Pendergrass SA, Sargent JL, George LK, McCalmont TH, Connolly MK, et al. Molecular subsets in the gene expression signatures of scleroderma skin [published correction appears in PloS One 2008;3] PLoS One 2008;7:3:e2696.

Mirizio E, Liu C, Yan Q, Waltermire J, Mandel R, Schollaert KL, et al. Genetic signatures from RNA sequencing of pediatric localized scleroderma skin. Front Pediatr 2021;9:669116.

Moon MS, Liu C, Fukuoka M, Dawood F, Chen M, Arab S, et al. Mindin, a regulator of innate immunity and inhibitor of angiogenesis, contributes to mortality and adverse remodeling post myocardial infarction. J Card Fail 2009;15:S39.

Murakoshi M, Gohda T, Tanimoto M, Funabiki K, Horikoshi S, Tomino Y. Role of mindin in diabetic nephropathy. Exp Diabetes Res 2011a 2011:486305.

Murakoshi M, Tanimoto M, Gohda T, Hagiwara S, Takagi M, Horikoshi S, et al. Mindin: a novel marker for podocyte injury in diabetic nephropathy. Nephrol Dial Transplant 2011b;26:2153–60.

Nakasaki M, Hwang Y, Xie Y, Kataria S, Gund R, Hajam EY, et al. The matrix protein Fibulin-5 is at the interface of tissue stiffness and inflammation in fibrosis. Nat Commun 2015;6:8574.

Noda S, Asano Y, Nishimura S, Taniguchi T, Fujiu K, Manabe I, et al. Simultaneous downregulation of KLF5 and Fli1 is a key feature underlying systemic sclerosis. Nat Commun 2014;5:5797.

Nowak JA, Fuchs E. Isolation and culture of epithelial stem cells. Methods Mol Biol 2009;482:215–32.

Oliveros JC, Venny. An interactive tool for comparing lists with Venn's diagrams. – References [Internet], Scientific Research Publishing. https://bioinfogp.cnb.csic.es/tools/venny/index.html; 2007.

Parry R, Schneider D, Hudson D, Parkes D, Xuan JA, Newton A, et al. Identification of a novel prostate tumor target, Mindin/RG-1, for antibody-based radiotherapy of prostate cancer. Cancer Res 2005;65:8397–405.

Pincha N, Hajam EY, Badarinath K, Batta SPR, Masudi T, Dey R, et al. PAI1 mediates fibroblast–mast cell interactions in skin fibrosis. J Clin Invest 2018a;128:1807–19.

Pincha N, Saha D, Bhatt T, Zirmire RK, Jamora C. Activation of fibroblast contractility via cell-cell interactions and soluble signals. Bio Protoc 2018b;8:e3021.

Qian X, Li C, Pang B, Xue M, Wang J, Zhou J. Spondin-2 (SPON2), a more prostate-cancer-specific diagnostic biomarker. PLoS One 2012;7:e37225.

Raja J, Denton CP. Cytokines in the immunopathology of systemic sclerosis. Semin Immunopathol 2015;37:543–57.

Rowe RG, Lin Y, Shimizu-Hirota R, Hanada S, Neilson EG, Greenson JK, et al. Hepatocyte-derived Snail1 propagates liver fibrosis progression. Mol Cell Biol 2011;31:2392–403.

Salmon-Ehr V, Serpier H, Nawrocki B, Gillery P, Clavel C, Kalis B, et al. Expression of interleukin-4 in scleroderma skin specimens and scleroderma fibroblast cultures. Potential role in fibrosis. Arch Dermatol 1996;132:802–6.

Sargent JL, Li Z, Aliprantis AO, Greenblatt M, Lemaire R, Wu MH, et al. Identification of optimal mouse models of systemic sclerosis by interspecies comparative genomics. Arthritis Rheumatol 2016;68:2003–15.

Schiopu E, Impens AJ, Phillips K. Digital ischemia in scleroderma spectrum of diseases. Int J Rheumatol 2010;2010:923743.

Schmid F, Wang Q, Huska MR, Andrade-Navarro MA, Lemm M, Fichtner I, et al. SPON2, a newly identified target gene of MACC1, drives colorectal cancer metastasis in mice and is prognostic for colorectal cancer patient survival. Oncogene 2016;35:5942–52.

Schuster R, Rockel JS, Kapoor M, Hinz B. The inflammatory speech of fibroblasts. Immunol Rev 2021;302:126–46.

Skaug B, Khanna D, Swindell WR, Hinchcliff ME, Frech TM, Steen VD, et al. Global skin gene expression analysis of early diffuse cutaneous systemic sclerosis shows a prominent innate and adaptive inflammatory profile. Ann Rheum Dis 2020;79:379–86.

Suliman YA, Bruni C, Johnson SR, Praino E, Alemam M, Borazan N, et al. Defining Skin Ulcers in Systemic Sclerosis: systematic Literature Review and Proposed World Scleroderma Foundation (WSF) definition. J Scleroderma Relat Disord 2017;2:115–20.

Sun P, Zhang P, Wang PX, Zhu LH, Du Y, Tian S, et al. Mindin deficiency protects the liver against ischemia/reperfusion injury. J Hepatol 2015;63:1198–211.

Takehara K, Sato S. Localized scleroderma is an autoimmune disorder. Rheumatol 2005;44:274–9.

Tighe RM, Potts EN, Feng F, Li Z, Frush B, He YW, et al. Extracellular matrix protein mindin is required for the complete allergic response to fungal-associated proteinase. J Allergy Ther 2011;2011:001.

Van Den Hoogen F, Khanna D, Fransen J, Johnson SR, Baron M, Tyndall A, et al. 2013 classification criteria for systemic sclerosis: an American College of Rheumatology/European League Against Rheumatism collaborative initiative. Ann Rheum Dis 2013;72:1747–55.

Wang IM, Zhang B, Yang X, Zhu J, Stepaniants S, Zhang C, et al. Systems analysis of eleven rodent disease models reveals an inflammatome signature and key drivers. Mol Syst Biol 2012;8:594.

Wang L, Lu Y, Zhang X, Zhang Y, Jiang D, Dong X, et al. Mindin is a critical mediator of ischemic brain injury in an experimental stroke model. Exp Neurol 2013;247:506–16.

Wick MJ, Harral JW, Loomis ZL, Dempsey EC. An optimized Evans blue protocol to assess vascular leak in the mouse. J Vis Exp 2018:57037.

Wigley FM, Flavahan NA. Raynaud's phenomenon. N Engl J Med 2016;375:556–65.

Wu B, Brooks JD. Gene expression changes induced by unilateral ureteral obstruction in mice. J Urol 2012;188:1033–41.

Wynn TA. Common and unique mechanisms regulate fibrosis in various fibroproliferative diseases. J Clin Invest 2007;117:524–9.

Wynn TA. Cellular and molecular mechanisms of fibrosis. J Pathol 2008;214:199–210.

Yang K, Li W, Bai T, Xiao Y, Yu W, Luo P, et al. Mindin deficiency alleviates renal fibrosis through inhibiting NF-κB and TGF-β/Smad pathways. J Cell Mol Med 2020;24:5740–50.

Yuan X, Bian T, Liu J, Ke H, Feng J, Zhang Q, et al. Spondin2 is a new prognostic biomarker for lung adenocarcinoma. Oncotarget 2017;8:59324–32.

Yue X, Yu X, Petersen F, Riemekasten G. Recent advances in mouse models for systemic sclerosis. Autoimmun Rev 2018;17:1225–34.

Zhang C, Qin JJ, Gong FH, Tong JJ, Cheng WL, Wang H, et al. Mindin deficiency in macrophages protects against foam cell formation and atherosclerosis by targeting LXR-β. Clin Sci (Lond) 2018;132:1199–213.

Zhang Q, Wang XQ, Wang J, Cui SJ, Lou XM, Yan B, et al. Upregulation of spondin-2 predicts poor survival of colorectal carcinoma patients. Oncotarget 2015;6:15095–110.

Zhu LH, Wang A, Luo P, Wang X, Jiang DS, Deng W, et al. Mindin/Spondin 2 inhibits hepatic steatosis, insulin resistance, and obesity via interaction with peroxisome proliferator-activated receptor α in mice. J Hepatol 2014 May;60(5):1046–54. https://doi.org/10.1016/j.jhep.2014.01.011.

SUPPLEMENTARY REFERENCE

Nakasaki M, Hwang Y, Xie Y, Kataria S, Gund R, Hajam EY, et al. The matrix protein Fibulin-5 is at the interface of tissue stiffness and inflammation in fibrosis. Nat Commun 2015;6:8574.

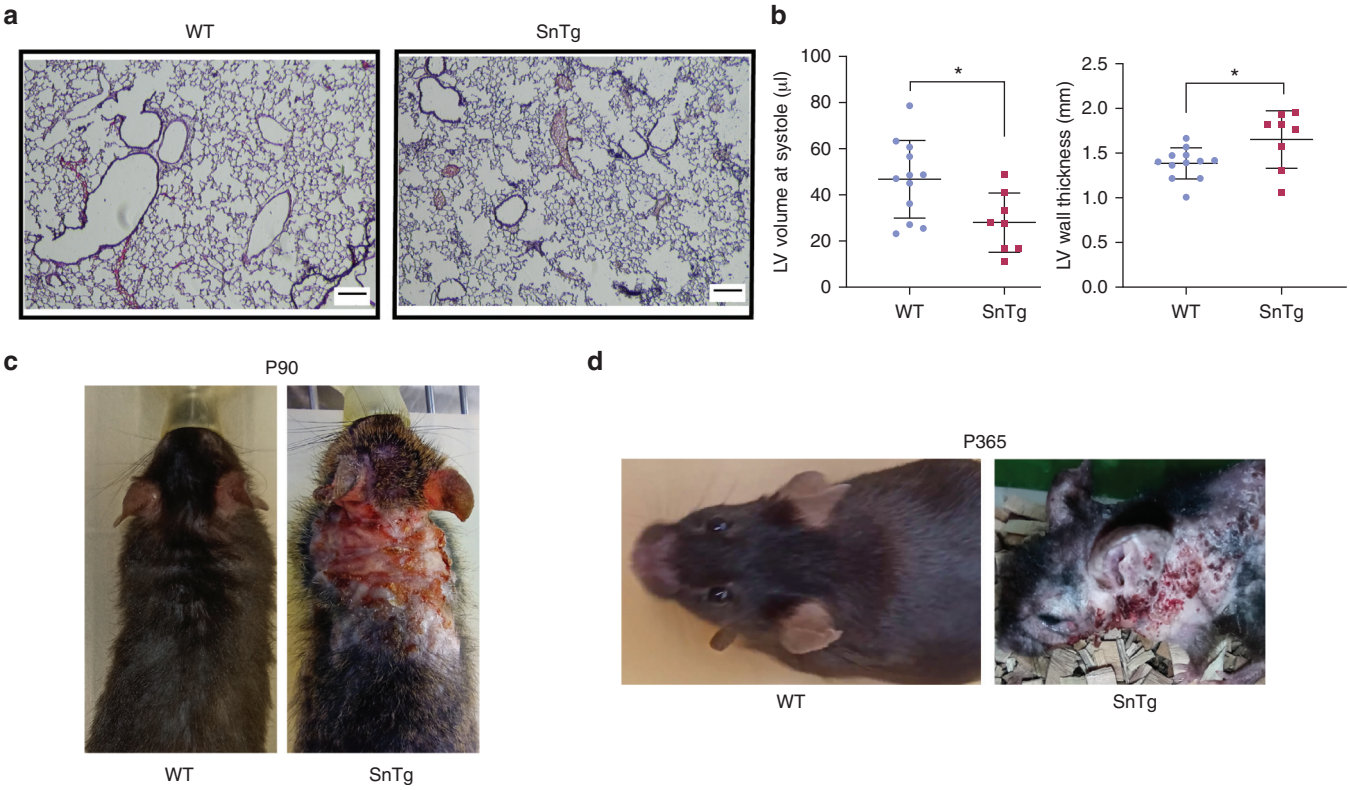

Supplementary Figure S1. SNAI1 Tg mouse model recapitulates diagnostic features of scleroderma. (**a**) H&E staining of lung sections taken from WT and SNAI1 Tg mice at P60. Bar = 200 µm. (**b**) Echocardiogram of the heart in WT and SNAI1 Tg mice aged 1 year. Comparison of values for LV volume at systole and LV wall thickness between WT (n = 12) and SNAI1 Tg (n = 8) mice. (**c**) Gross appearance of the skin lesions observed at the dorsal neck area of the adult (P90) SNAI1 Tg mice (right panel) compared with that of the WT (P90) mice (left panel). (**d**) Gross appearance of the skin lesions observed at the dorsal neck area of SNAI1 Tg mice aged 1 year (right panel) compared with that of the WT (P90) mice (left panel). The error bars represent mean ± SEM. *P*-value was calculated by (**b**) Welch's *t* test. $*P < 0.05$. LV, left ventricular; P365, postnatal day 360; P60, postnatal day 60; P90, postnatal day 90; SnTg, SNAI1 transgenic; Tg, transgenic; WT, wild type.

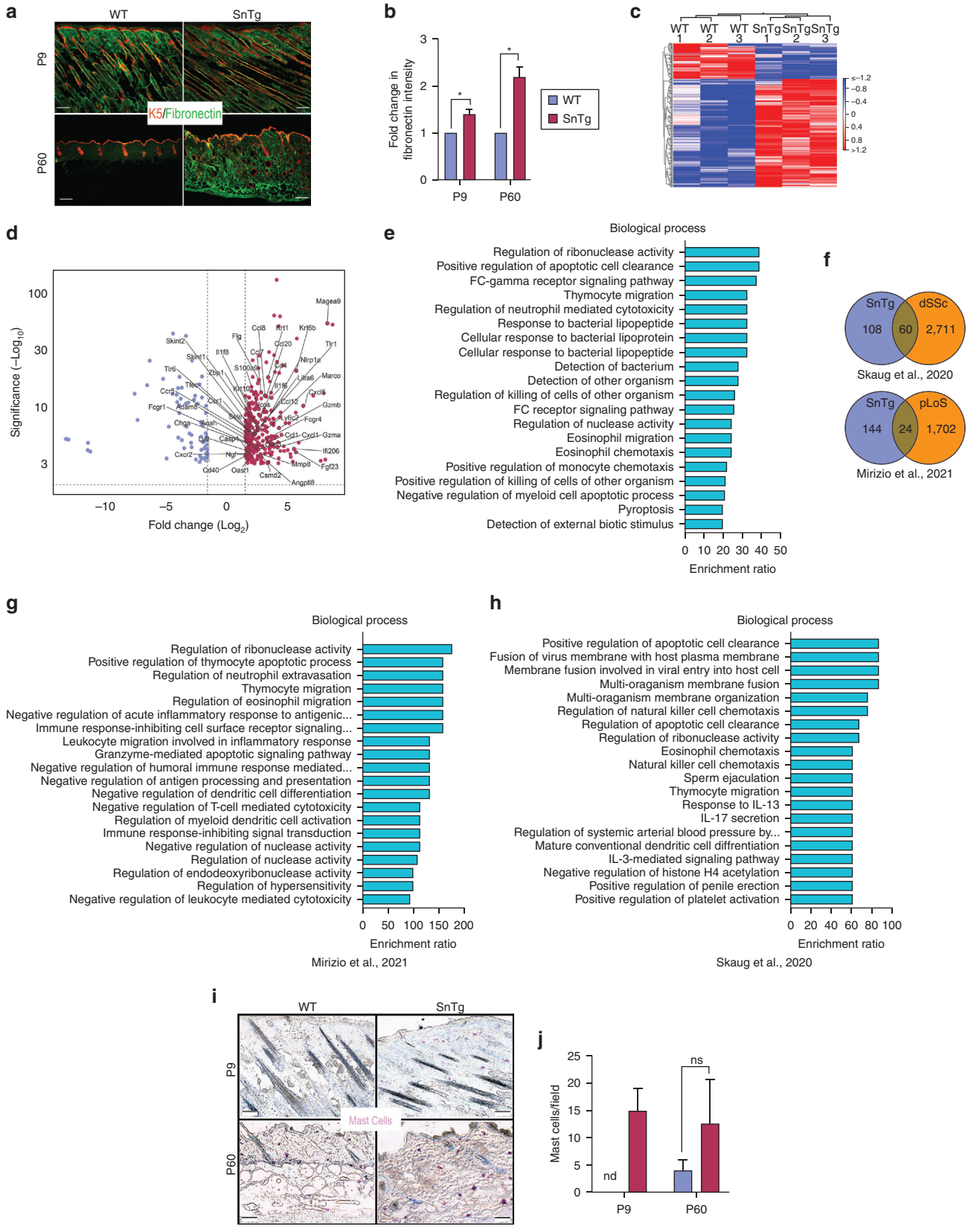

Supplementary Figure S2. SNAI1 Tg mice recapitulate histological and molecular characteristics of SSc. (**a**) Immunofluorescence imaging for K5 (red) and fibronectin (green) in WT and SNAI1 Tg mice at P9 and P60. Bar = 100 μm. (**b**) Quantification of dermal fibronectin staining in P9 WT (n = 4) and SNAI1 Tg (n = 4) and P60 WT (n = 5) and SNAI1 Tg (n = 5) mice (two microscopic fields per mouse were analyzed). (**c**) Heatmap of differentially regulated genes in P9 WT (n = 3) and SNAI1 Tg (n = 3) mice. Red = upregulated, blue = downregulated. (**d**) Volcano plot of upregulated and downregulated genes. (**e**) Biological processes based on GO term enrichment of genes upregulated in the skin of the SNAI1 Tg mice. (**f**) Comparison between upregulated genes of P9 SNAI1 Tg mice with upregulated genes from patients with SSc in GEO dataset (GSE130955 [Skaug et al., 2020], diffused scleroderma) and (GSE166861 [Mirizio et al., 2021],

pediatric localized scleroderma). (**g**) Biological processes based on GO term enrichment of upregulated genes common in the skin of the SNAI1 Tg mice and SSc (GSE166861 [Mirizio et al., 2021], pediatric localized scleroderma). (**h**) Biological processes based on GO term enrichment of upregulated genes common in the skin of the SNAI1 Tg mice and SSc (GSE130955 [Skaug et al., 2020], diffused scleroderma). (**i**) Toluidine blue staining for mast cells in WT and SNAI1 Tg at P9 and P60. Bar = 50 μm. (**j**) Quantification of the number of mast cells per microscopic field in P9 WT (n = 3) and SNAI1 Tg (n = 3), P60 WT (n = 3), and SNAI1 Tg (n = 3) mice. The error bars represent mean ± SEM. *P*-value was calculated using (**j**) two-tailed Welch's *t* test and (**a**) ratio-paired *t* test. *$P < 0.05$. ns, $P > 0.05$. GEO, Gene Expression Omnibus; GO, Gene Ontology; K5, keratin 5; nd, not detected; ns, ns, nonsignificant; P60, postnatal day 60; P9, postnatal day 9; SnTg, SNAI1 transgenic; SSc, systemic sclerosis; Tg, transgenic; WT, wild type.

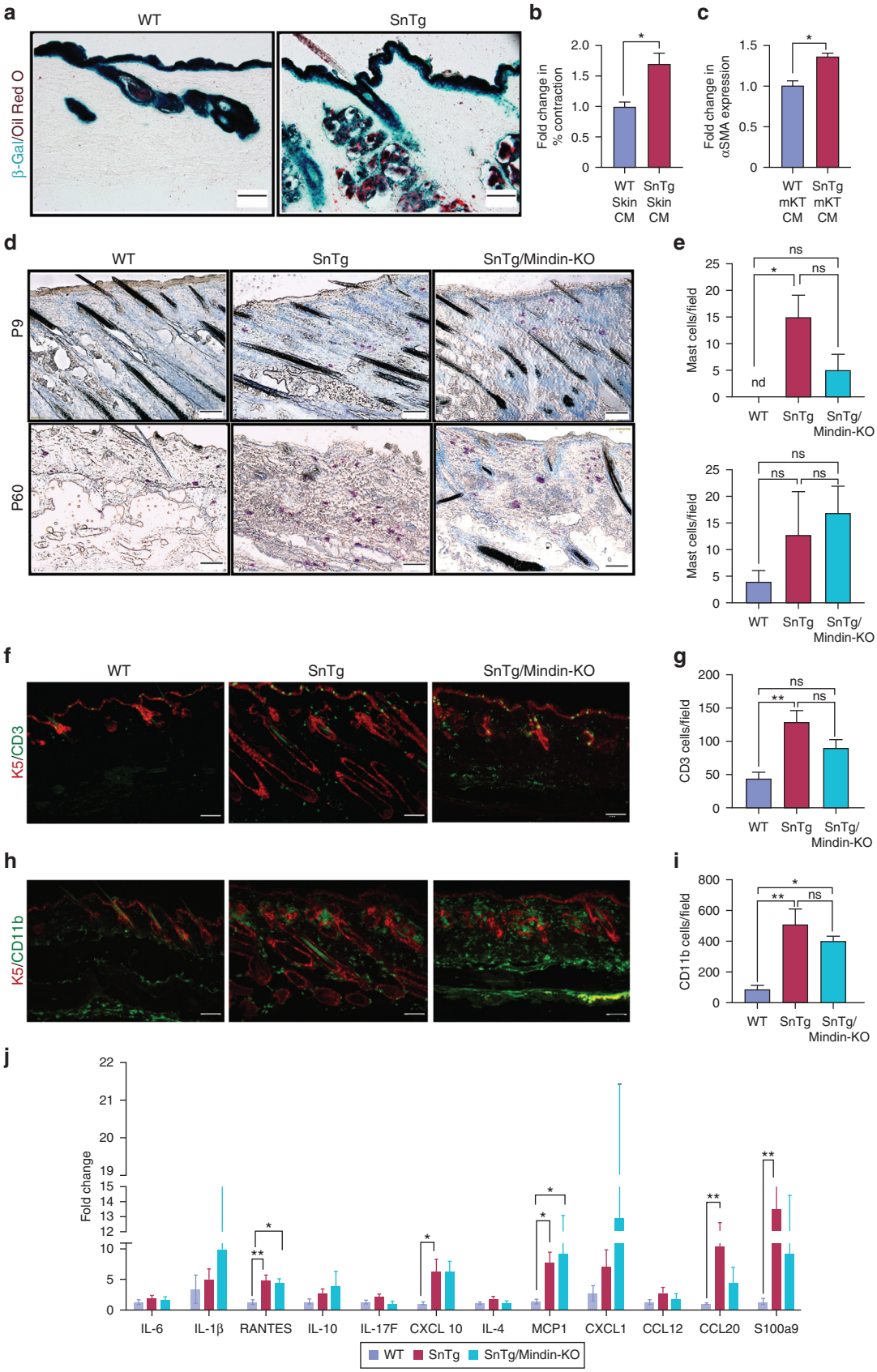

Supplementary Figure S3. Secreted Mindin leads to fibrotic phenotype. (**a**) Lineage tracing of the WT and SNAI1 Tg mice using the K14-Cre R26R reporter. All cells of epithelial origin are positive for β-Gal (blue), and oil red O marks the sebaceous glands (red). Bar = 50 μm. (**b**) CM was collected from WT (n = 3) and SNAI1 Tg (n = 3) mouse skin explants. Fibroblast activation was measured with the collagen contraction assay. (**c**) αSMA gene expression to assess fibroblast activation after treatment with WT and SNAI1 Tg keratinocytes CM. (**d**) Mast cells (purple) staining in WT, SNAI1 Tg, and SNAI1 Tg/Mindin-KO at P9 and P60.

Bar = 50 μm. (**e**) Quantification of the number of mast cells per microscopic field in P9 WT (n = 3), SNAI1 Tg (n = 3), SNAI1 Tg/Mindin-KO (n = 3) and P60 WT (n = 3), SNAI1 Tg (n = 3), and SNAI1 Tg/Minding-KO (n = 3) mice. Two microscopic fields per mouse were counted. WT and SNAI1 Tg for P9 and P60 data are the same as used earlier for Supplementary Figure 2j. (**f**) T cells in WT, SNAI1 Tg, and SNAI1 Tg/Minding-KO mice skin at P60. Skin sections were stained for K5 (red) and T cells (CD3, green). Bar = 100 μm. (**g**) Quantification of the number of $CD3^+$ cells per microscopic field in P60 WT (n = 3), SNAI1 Tg (n = 3), and SNAI1 Tg/Minding-KO (n = 3) mice. Two microscopic fields per mouse were counted. WT and SNAI1 Tg data are the same as in Figure 2j. (**h**) $CD11b^+$ cells in WT, SNAI1 Tg, and SNAI1 Tg/Mindin-KO mice skin at P60. Skin sections were stained for K5 (red) and CD11b (green). Bar = 100 μm. (**i**) Quantification of the number of $CD11b^+$ cells per microscopic field in P60 WT (n = 3), SNAI1 Tg (n = 3), and SNAI1 Tg/Mindin-KO (n = 3) mice. Two microscopic fields per mouse were counted. WT and SNAI1 Tg data are the same as in Figure 2h. (**j**) qPCR for inflammatory cytokines gene expression in WT (n = 9), SNAI1 Tg (n = 7), and SNAI1 Tg/Mindin-KO (n = 3) skin at P60. WT (P60) and SNAI1 Tg (P60) are the same samples used earlier for Figure 2f. The error bars represent mean ± SEM. *P*-value was calculated using (**b, c**) two-tailed Welch's *t* test and (**e, g, i, j**) one-way ANOVA followed Tukey's posthoc analysis for multiple-group comparison. $*P < 0.05$, $**P < 0.01$, $***P < 0.001$, and $****P < 0.0001$. αSMA, α-smooth muscle actin; β-Gal, galactosidase; CM, conditioned media; K5, keratin 5; KO, knockout; P60, postnatal day 60; P9, postnatal day 9; SnTg, SNAI1 transgenic; Tg, transgenic; WT, wild type.

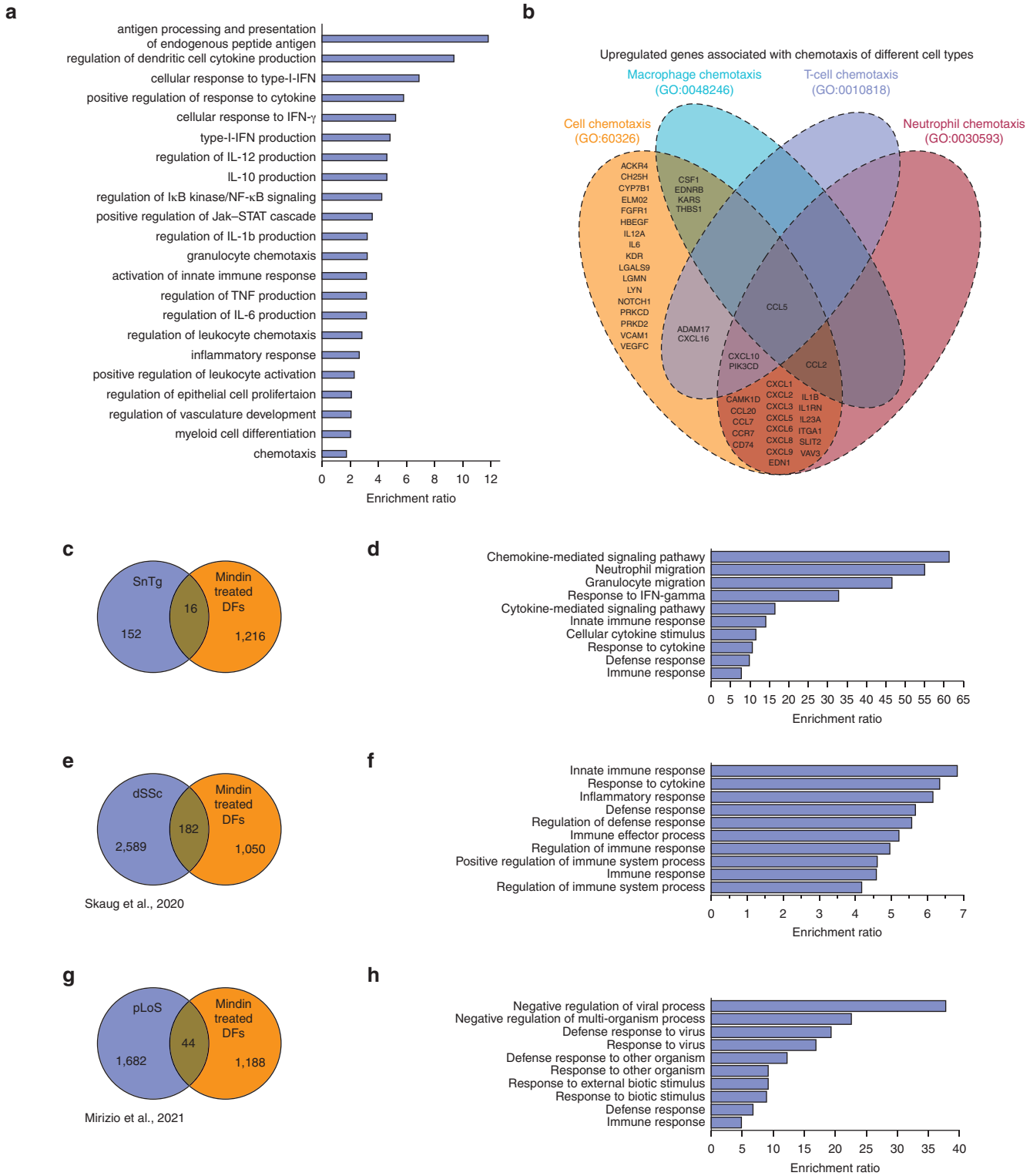

Supplementary Figure S4. Mindin-treated fibroblasts show an overlap with SNAI1 Tg mice and human SSc. (**a**) Biological processes based on GOTERM enrichment of genes upregulated in fibroblasts treated with Mindin. (**b**) Venn diagram of upregulated genes in Mindin-treated fibroblasts that are involved in chemotaxis of immune cells. (**c**) Venn diagram of overlapping upregulated genes in SNAI1 Tg mice and Mindin-treated fibroblasts. (**d**) Top 10 biological processes of GOTERMS of upregulated genes that are held in common in SNAI1 Tg mice and Mindin-treated fibroblasts. (**e**) Venn diagram of overlapping upregulated genes in patients with early dSSc (GSE130955 [Skaug et al., 2020]) and Mindin-treated fibroblasts. (**f**) Top 10 biological processes of GOTERMS of upregulated genes that are held in common in dSSc and Mindin-treated fibroblasts. (**g**) Venn diagram of overlapping upregulated genes in patients with early pLoS (GSE166861 [Mirizio et al., 2021] and Mindin-treated fibroblasts. (**h**) Top 10 biological processes of GOTERMS of upregulated genes that are held in common in pediatric limited SSc and Mindin-treated fibroblasts. DF, dermal fibroblasts; dSSc, diffused systemic sclerosis; GOTERMS, Gene Ontology Terms; pLoS, pediatric localized scleroderma; SSc, systemic sclerosis; STAT, signal transducer and activator of transcription; Tg, transgenic.

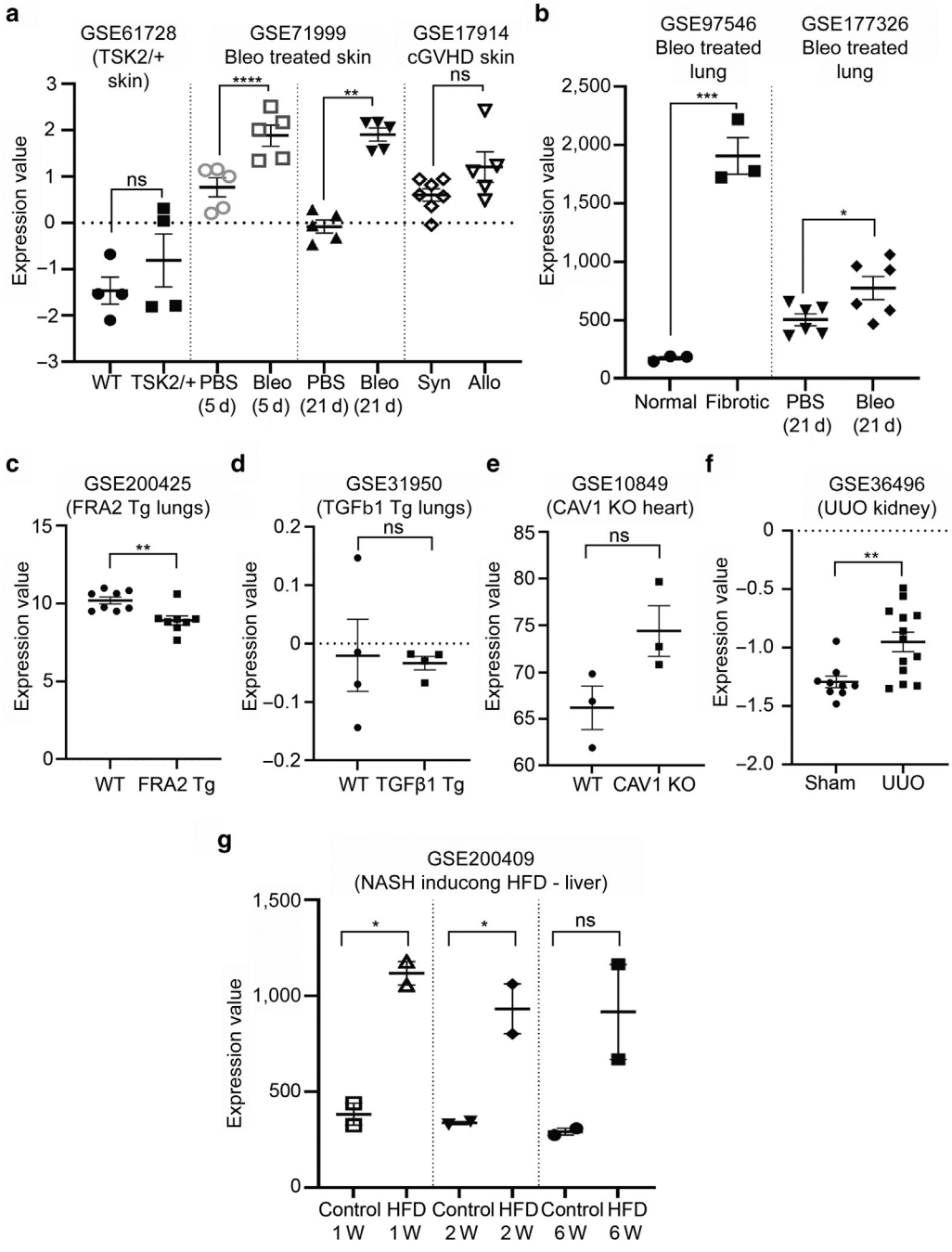

Supplementary Figure S5. Mindin is overexpressed in other mouse models of fibrosis. (**a**) Expression values for Mindin in the skin of WT and TSK2/+ (GSE61728); 5 d and 21 d post-PBS or -bleomycin treatment (GSE71999); Syn- and Allo-transplanted cGVHD model (GSE17914). (**b**) Expression values for Mindin in normal versus Fibrotic lungs (treated with bleomycin) (GSE97546) and in lungs of mice treated with either PBS or bleomycin (21 d after treatment). (**c**) Expression values for Mindin in lungs of WT and FRA Tg mice. (**d**) Expression values for Mindin in the lungs of WT and TGFβ1 Tg mice. (**e**) Expression values for Mindin in the heart of WT and caveolin-1–knockout mice. (**f**) Expression values for Mindin in the kidney of WT and knockout mice that underwent either sham or UUO surgery. (**g**) Expression values for Mindin in the liver of mice given either control or NASH-inducing high-fat diet. Allo, allogenic; Bleo, bleomycin; cGVHD, chronic graft-versus-host disease; d, day; HFD, high-fat diet; KO, knockout; NASH, non-alcoholic steatohepatitis; ns, nonsignificant; Syn, syngeneic; Tg, transgenic; UUO, unilateral ureteral obstruction; W, week; WT, wild type.

Supplementary Table S1. ANA Staining Results of WT, SnTg, and SnTg/Min KO for dilutions 1:10 to 1:200

Dilution Factor	1:10	1:25	1:50	1:100	1:200
WT-1	–	–	–	–	–
WT-2	–	–	–	–	–
WT-3	–	–	–	–	–
WT-4	–	–	–	–	–
WT-5	–	–	–	–	–
WT-6	–	–	–	–	–
WT-7	–	–	–	–	–
WT-8	–	–	–	–	–
SnTg-1	+	+	+	+	+
SnTg-2	–	–	–	–	–
SnTg-3	+	+	+	+	+
SnTg-4	+	+	+	+	–
SnTg-5	+	+	+	+	+
SnTg-6	–	–	–	–	–
SnTg-7	+	+	+	+	+
SnTg-8	+	+	+	+	+
SnTg/Min KO-1	–	–	–	–	–
SnTg/Min KO-2	–	–	–	–	–
SnTg/Min KO-3	+	+	+	+	+
SnTg/Min KO-4	–	–	–	–	–

Abbreviations: ANA, antinuclear antibody; KO, knockout; Sn, snail; Tg, transgenic; WT, wild type.

Shown are ANA staining results of WT, SNAI1 Tg, and SNAI1 Tg/Mindin-KO for dilutions 1:10 to 1:200. The + sign represents positive staining, and the – sign represents negative staining.

Supplementary Table S2. Summary of SSc-Associated Phenotypes

P9	Sample Size	Raynaud's Phenomenon in Tail[1]	Puffy Paws/ Tail[1]	Skin Lesions on Tail	Tail Tip Ischemic Ulcer[1]
WT	17	0/17	0/17	0/17	0/17
Snail Tg	6	5/6	4/6	5/6	3/6
Snail Tg/ Min KO	5	2/5	1/5	4/5	2/5

P60	Sample Size	Raynaud's Phenomenon in Tail[1]	ANA[1,2]	Puffy Paws[1]	Tail Autoamputation
WT	8	0/8	0/6	0/8	0/8
Snail Tg	9	8/9	4/7	4/9	9/9
SnailTg/ Min KO	5	2/5	1/4	1/5	2/5

Abbreviations: ACR-EULAR, European League Against Rheumatism and the American College of Rheumatology; ANA, antinuclear antibody; KO, knockout; P60, postnatal day 60; P9, postnatal day 9; SSC, systemic sclerosis; Tg, transgenic; WT, wild type.

The number of mice exhibiting the noted symptom/the total number of mice observed is shown.

[1]Symptom similar to ACR-EULAR diagnostic criteria.

[2]Animals that showed nuclear localization in 1:10 dilution of Sera were counted as positive.

Supplementary Table S3. A Tabulated Representation of Cytokine Gene Expression Levels

	P9			P60			WT vs SnTg CM		Buffer vs Mindin	
Gene	**WT**	**SnTg**	**SnTg/MinKO**	**WT**	**SnTg**	**SnTg/MinKO**	**WT-CM**	**SnTg CM**	**Buffer**	**Mindin**
IL-6	1.56 ± 0.49	6.44 ± 1.57[1]	3.22 ± 0.79[ns]	1.12 ± 0.2	2.0 ± 0.4[ns]	1.72 ± 0.49[ns]	1.01 ± 0.11	2.72 ± 0.19[2]	1 ± 0.05	1.03 ± 0.04[ns]
IL-1b	1.43 ± 0.53	14.47 ± 3.05[3]	5.97 ± 2.28[ns]	3.46 ± 2.34	5.14 ± 1.6[ns]	10.08 ± 8.42[ns]	1.03 ± 0.17	0.12 ± 0.03[1]	1 ± 0.02	15.64 ± 0.87[2]
RANTES	1.25 ± 0.33	5.18 ± 1.28[1]	6.79 ± 2.29[ns]	1.3 ± 0.39	4.92 ± 0.85[2]	4.53 ± 0.61[ns]	1.02 ± 0.15	0.6 ± 0.01[ns]	1 ± 0.05	4.93 ± 0.49[1]
IL-17F	2.19 ± 0.76	7.17 ± 2.8[ns]	3.93 ± 2.09[ns]	1.33 ± 0.32	2.27 ± 0.35[ns]	1.05 ± 0.41[ns]	1.05 ± 0.22	1.73 ± 0.13[ns]	1.01 ± 0.08	0.67 ± 0.02[1]
IL-4	1.67 ± 0.43	7.31 ± 2.57[ns]	5.58 ± 1.77[ns]	1.14 ± 0.21	1.97 ± 0.31[ns]	1.21 ± 0.34[ns]	1.05 ± 0.22	1.29 ± 0.05[ns]	1 ± 0.03	0.73 ± 0.03[2]
CXCL1	1.91 ± 0.67	26.59 ± 5.55 8[3]	0.75 ± 0.33[2]	2.74 ± 1.29	7.19 ± 2.68[ns]	12.91 ± 8.52[ns]	1.05 ± 0.24	2.41 ± 0.12[1]	1 ± 0.04	11.45 ± 0.47[2]
CCL12	1.47 ± 0.4	4.2 ± 0.55[2]	3.84 ± 0.27[ns]	1.29 ± 0.34	2.91 ± 0.79[ns]	1.85 ± 0.82[ns]	1.00 ± 0.02	0.1 ± 0.01[3]	1 ± 0.05	3.58 ± 0.41[1]
CCL20	1.66 ± 0.53	13.88 ± 2.46[4]	5.02 ± 0.95[1]	1.07 ± 0.12	10.47 ± 2.14[3]	4.49 ± 2.51[ns]	1.03 ± 0.19	0.06 ± 0[1]	1.04 ± 0.19	27.1 ± 0.32[4]
S100a9	1.48 ± 0.5	15.44 ± 5.15[1]	4.38 ± 2.09[ns]	1.44 ± 0.53	13.48 ± 2.75[2]	9.2 ± 5.23[ns]	ND	ND	ND	ND

Abbreviations: CM, conditioned media; KO, knock out; ND, not detected; NS, not significant; P60, postnatal day 60; P9, postnatal day 9; SnTg, snail Tg; SnTg/MinKO, Snail Tg/Mindin KO; WT, wild type.

Expression levels were shown as average fold change ± SEM in P9 WT (n = 8) , SnTg (n ≥ 6), and SnTg/MinKO (n = 3); P60 WT (n = 9), SnTg (n = 7), and SnTg/MinKO (n = 3); WT-CM (n = 3 biological replicates) versus SnTg-CM (n = 3 biological replicates); and Buffer versus Mindin (n = 3 technical replicates). *P*-values were calculated using one-way ANOVA followed by post hoc Tukey's test for P9 and P60 (significance values were shown as superscripts for WT vs. SnTg and SnTg vs. SnTg/MinKO for significance values of WT vs. SnTg/MinKO) (Figure 3i and Supplementary Figure S3j) and Welch's *t* test for WT versus SnTg-CM and Buffer versus Mindin (significance values were shown as superscripts).

[1] $P < 0.05$.

[2] $P < 0.01$.

[3] $P < 0.001$.

[4] $P < 0.0001$.

Supplementary Table S4. List of Primers Used for qPCR

Quantitative Real-time PCR Primers

Gene	Forward Primer	Reverse Primer
m_GAPDH	AGGTCGGTGTGAACGGATTTG	TGTAGACCATGTAGTTGAGGTCA
m_b Actin	GGGCTATGCTCTCCCTCAC	GATGTCACGCACGATTTCC
m_Snail	CAGCTGGCCAGGCTCTCGGT	GCGAGGGCCTCCGGAGCA
m_Mindin	ATGGAAAACGTGAGTCTTGCC	TGATGCTGTATCTAGCCAGAGG
m_IL 6	ACAACCACGGCCTTCCCTACTT	CACGATTTCCCAGAGAACATGTG
m_IL 1b	TGCCACCTTTTGACAGTGATG	TGATGTGCTGCTGCGAGATT
m_RANTES	CCTCACCATCATCCTCACTGCA	TCTTCTCTGGGTTGGCACACAC
m_IL 10	GGCGCTGTCATCGATTTCTC	ATGGCCTTGTAGACACCTTGG
m_IL 17 F	CAGACACTCAGGCTGCATCA	TGGACAATGGGCTTGACACA
m_CXCL 10	CCAAGTGCTGCCGTCATTTTC	GGCTCGCAGGGATGATTTCAA
m_IL 4	GGTCTCAACCCCCAGCTAGT	GCCGATGATCTCTCTCAAGTGAT
m_MCP1	ACTGAAGCCAGCTCTCTCTTCCTC	TTCCTTCTTGGGGTCAGCACAGAC
m_CXCL 1	ACTGCACCCAAACCGAAGTC	TGGGGACACCTTTTAGCATCTT
m_CCL 12	ATTTCCACACTTCTATGCCTCCT	ATCCAGTATGGTCCTGAAGATCA
m_CCL 20	AGGCAGAAGCAGCAAGCAAC	ACAAGCTTCATCGGCCATCT
m_S100A9	ATACTCTAGGAAGGAAGGACACC	TCCATGATGTCATTTATGAGGGC
m_*αSMA*	ATCGTCCACCGCAAATGC	AAGGAACTGGAGGCGCTG
h_GAPDH	GCCACATCGCTCAGACAC	CCAGAGTTAAAAGCAGCC
h_b Actin	TCCTTCCTGGGCATGGAGT	AGCACTGTGTTGGCGTACAG
h_Snail	ACCACTATGCCGCGCTCTT	GGTCGTAGGGCTGCTGGAA
h_Mindin	CGCTGGACCTGTACCCCTA	AGGAGGACGTTATCTCGGTCA

Supplementary Table S5. Scleroderma Patient Information

Biopsy Number	Age, y	Sex	Disease Duration	Modified Rodnan Skin Score
SSC 5	41	F	2 y	36
SSC 212	34	F	3 y	47
SSC 166	31	F	1.5 y	42
SSC 116	45	M	6 mo	41
SSC 111	44	M	1.5 y	8
SSC 8	46	M	2 y	32
SSC 7	48	F	3 y	44
SSC 6	43	M	1 y	26
SSC 4	45	M	1 y	45
SSC 3	40	F	4 mo	22
SSC 299	42	F	6 mo	21
SSC 214	36	F	2.5 y	32

Abbreviations: F, female; M, male; SSC, systemic sclerosis.

Healthy skin samples were collected from healthy humans with same age and sex. These samples were the same as those used in Nakasaki et al. (2015).